







ORIGINAL RESEARCH

Dysregulated Genes, MicroRNAs, Biological Pathways, and Gastrocnemius Muscle Fiber Types Associated With Progression of Peripheral Artery Disease: A Preliminary Analysis

Sunil K. Saini , PhD*; Daniel Pérez-Cremades , PhD*; Henry S. Cheng, PhD*; Kate Kosmac, PhD; Charlotte A Peterson , PhD; Lingyu Li, MS; Lu Tian, ScD; Gengfu Dong , BS, MS; Kevin K. Wu, MD; Brian Bouverat, MS; Stephanie E. Wohlgemuth, PhD; Terence Ryan , PhD; Robert L. Sufit , MD; Luigi Ferrucci , MD, PhD; Mary M. McDermott , MD; Christiaan Leeuwenburgh , PhD; Mark W. Feinberg , MD

BACKGROUND: Peripheral artery disease (PAD) is associated with gastrocnemius muscle abnormalities. However, the biological pathways associated with gastrocnemius muscle dysfunction and their associations with progression of PAD are largely unknown. This study characterized differential gene and microRNA (miRNA) expression in gastrocnemius biopsies from people without PAD compared with those with PAD. Participants with PAD included those with and without PAD progression.

METHODS AND RESULTS: mRNA and miRNA sequencing were performed to identify differentially expressed genes, differentially expressed miRNAs, mRNA-miRNA interactions, and associated biological pathways for 3 sets of comparisons: (1) PAD progression (n=7) versus non-PAD (n=7); (2) PAD no progression (n=6) versus non-PAD; and (3) PAD progression versus PAD no progression. Immunohistochemistry was performed to determine gastrocnemius muscle fiber types and muscle fiber size. Differentially expressed genes and differentially expressed miRNAs were more abundant in the comparison of PAD progression versus non-PAD compared with PAD with versus without progression. Among the top significant cellular pathways in subjects with PAD progression were muscle contraction or development, transforming growth factor-beta, growth/differentiation factor, and activin signaling, inflammation, cellular senescence, and notch signaling. Subjects with PAD progression had increased frequency of smaller Type 2a gastrocnemius muscle fibers in exploratory analyses.

CONCLUSIONS: Humans with PAD progression exhibited greater differences in the number of gene and miRNA expression, biological pathways, and Type 2a muscle fiber size compared with those without PAD. Fewer differences were observed between people with PAD without progression and control patients without PAD. Further study is needed to confirm whether the identified transcripts may serve as potential biomarkers for diagnosis and progression of PAD.

Key Words: differentially expressed genes (DEG) ■ gastrocnemius muscle ■ peripheral artery disease (PAD)

Correspondence to: Mark W. Feinberg, MD, Brigham and Women's Hospital and Harvard Medical School, 75 Francis St, Boston, MA 02115. Email: mfeinberg@bwh.harvard.edu and Christiaan Leeuwenburgh, PhD, University of Florida, Office CTRB 3125, 2004 Mowry Rd, PO Box 100107, Gainesville, FL 32611. Email: cleeuwen@ufl.edu

*S. K. Saini, D. Pérez-Cremades, and H. S. Cheng contributed equally.

Supplemental Material is available at <https://www.ahajournals.org/doi/suppl/10.1161/JAHA.121.023085>

For Sources of Funding and Disclosures, see page 14.

© 2022 The Authors. Published on behalf of the American Heart Association, Inc., by Wiley. This is an open access article under the terms of the [Creative Commons Attribution-NonCommercial-NoDerivs](#) License, which permits use and distribution in any medium, provided the original work is properly cited, the use is non-commercial and no modifications or adaptations are made.

JAHA is available at: www.ahajournals.org/journal/jaha

CLINICAL PERSPECTIVE

What Is New?

- Patients with peripheral artery disease (PAD) who had functional decline over 6 months exhibited differences in gene and microRNA expression, signaling pathways, and Type 2a muscle fiber size compared with subjects with non-PAD.
- Among the top significant cellular pathways and transcripts in subjects with PAD and functional decline were muscle contraction or development, transforming growth factor-beta, growth/differentiation factor, and activin signaling, inflammation, cellular senescence, and notch signaling.

What Are the Clinical Implications?

- Our findings highlight the potential of global profiling of gene and microRNA expression in identifying transcripts that could serve as potential biomarkers of progression of PAD.
- Further studies are needed to confirm these findings and validate the clinical utility of the biomarkers associated with functional decline in PAD.

Nonstandard Abbreviations and Acronyms

CDKN1A	cyclin dependent kinase inhibitor 1A
DEG	differentially expressed genes
GDF	growth/differentiation factor
LIMK1	LIM domain kinase 1
miRNA	microRNA
miRNA-Seq	microRNA sequencing
MYBPH	myosin binding protein H
MyHC	myosin heavy chain
MYL5	myosin light chain 5
MYL6	myosin light chain 6
NNMT	nicotinamide N-methyltransferase
OXCT1	3-oxoacid CoA-transferase 1
RT-qPCR	real-time quantitative PCR
S100A8	S100 calcium binding protein A8
S100A9	S100 calcium binding protein A9
TGFβ	transforming growth factor-beta

Lower extremity peripheral artery disease (PAD) causes ischemia of the lower extremities and is associated with gastrocnemius muscle abnormalities, including increased oxidative stress,^{1,2} increased apoptosis,³ altered skeletal muscle morphology and metabolism,^{2,4} and reduced mitochondrial respiration.^{5,6} Some

pathophysiological changes in gastrocnemius muscle, such as smaller fiber size and oxidative stress, have been associated with greater functional impairment and mobility loss in people with PAD.⁷⁻⁹ Identifying the biological pathways associated with impaired gastrocnemius muscle function and progression of PAD may lead to new effective strategies that can reverse calf muscle dysfunction and improve mobility in people with PAD.

Advancement in high throughput sequencing techniques facilitates profiling whole transcriptomes, including gene and microRNA (miRNA)¹⁰ expression, and making inferences about biological pathways that are affected by diverse pathophysiological conditions in different cell types. miRNAs are short, single-stranded, noncoding RNAs that post-transcriptionally regulate expression of ~60% of all mammalian protein encoding genes and can also more broadly impact RNA metabolism and translation.¹¹ In most cases, miRNA binding to mRNAs results in mRNA degradation and/or inhibition of translation, regulating a diverse range of developmental, physiological, and disease processes, including stem cell differentiation, hypoxia, cardiac and skeletal muscle development, aging, and mitochondrial function.¹² A recent study has identified miR-323b-5p as a potential biomarker of critical chronic limb ischemia in patients with diabetes.¹⁰ However, the full spectrum of miRNAs dysregulated specifically in gastrocnemius muscles with progression of PAD is poorly understood. Several basic biological mechanisms may be dysregulated in PAD (ie, lower extremity skeletal muscle differentiation, muscle development, extracellular matrix remodeling, autophagy, among others) because of repeated episodes of ischemia/reperfusion, both through direct effects on mRNA transcription and through changes in miRNA.

The purpose of this study was to identify protein coding genes and miRNA transcripts in gastrocnemius muscle biopsies that are differentially expressed in PAD versus controls free of PAD. A case control design was used to identify skeletal muscle transcripts and muscle fiber types associated with clinical progression of PAD versus absence of PAD progression in people with PAD matched by sex and race who were followed longitudinally.

METHODS

Data Availability

The data, methods used in the analysis, and materials used to conduct the research of this study are available from the corresponding authors upon reasonable request.

Participant Recruitment

Muscle specimens for participants with PAD were obtained from participants in observational studies or

randomized trials.^{13–15} Participants without PAD were identified from either longitudinal observational studies or clinical trials comparing muscle characteristics between people with and without PAD, and participants with PAD were identified from participants eligible for a randomized trial who had a baseline muscle biopsy. Participants were categorized into 1 of 3 groups: People without PAD, people with PAD who developed disease progression (defined as people with PAD who experienced meaningful decline in 6-minute walk [>25 meters] between baseline and 6-month follow-up) and people with PAD who did not experience disease progression. Groups of muscle biopsies, matched by race and sex, were identified that included 1 participant with PAD without progression, 1 participant with PAD with progression, and 1 participant without PAD. For each group of 3 muscle biopsies, when there was >1 possible muscle match based on sex and race, the individual closest in age was selected. Participants with PAD who received a therapeutic intervention in a randomized trial between baseline and 6-month follow-up were not eligible for this study. Overall, 20 calf muscle biopsy specimens from 20 participants (7 PAD progression, 6 PAD no progression, and 7 non-PAD) were included. The Institutional Review Board at Northwestern University approved each study protocol. All participants provided written informed consent. Recruitment methods included postcards mailed to older people in the Chicago area; Chicago Transit Authority advertisements; identification of individuals who had previously participated in research studies with the principal investigator (M.M.M.) at Northwestern and had expressed interest in future research participation; physician referral; through mailed letters at the Veterans Administration; and newspaper advertisements.

Inclusion and Exclusion Criteria

Inclusion and exclusion criteria for the biobank with the principal investigator (M.M.M.) at Northwestern were reported previously^{13,16} and are briefly summarized here. PAD was defined as a resting ankle brachial index (ABI) <0.90 , those with ABI of 0.90 to 1.00 who experience a 20% or higher drop in ABI after heel-rise exercise during a study visit, or evidence of PAD from vascular laboratory testing. Participants with PAD whose walking was primarily limited by a comorbidity other than PAD were excluded. Participants with below-knee or above-knee amputation, wheel-chair confinement, use of a walking aid, significant visual or hearing impairment, and any recent major surgery were excluded. Participants with non-PAD had a resting ABI of 1.0–1.40 with no history of PAD.

Measurement of ABI

ABI was measured using a handheld Doppler probe (Nicolet Vascular Pocket Dop II, Golden, CO) as

described previously.^{17,18} Briefly, systolic blood pressure was measured twice in the right and left brachial, dorsalis pedis, and posterior tibial arteries, respectively. The ABI was calculated as the ratio of the average systolic pressure of the dorsalis pedis and posterior tibial in each leg divided by the mean of the 4 systolic brachial pressures. Mean systolic pressure in the arm with the higher pressure was used when 1 brachial pressure was higher than the opposite brachial pressure in both measurement sets and the 2 brachial pressures differed by ≥ 10 mmHg in one measurement set.¹⁹

Six-Minute Walk Test

The 6-minute walk test was performed according to previously reported methods.¹³ Briefly, participants were asked to walk up and down in a 100-foot hallway for 6 minutes to cover as much distance as possible, and the total distance covered in 6 minutes was recorded.

Four-Meter Walking Velocity

Walking velocity for a 4-m walk was measured both at “usual” and “fastest” pace. Participants were asked to walk at their normal pace as if they were “walking down the street to go to the store” and separately to walk as fast as they could for 4 m. Each walk was performed twice, and the fastest velocity was used for each measure.¹⁸

Other Characteristics

Comorbidities, including diabetes, were identified based on participant self-report, using standardized data collection forms. Race was identified based on self-report, using categories defined by National Institutes of Health reporting standards. Height and weight were measured at the study visit. BMI was calculated as weight (kg)/height (m²).

Muscle Biopsy Procedure

All participants underwent open biopsy in the medial head of the gastrocnemius muscle. Anesthesia was attained with subcutaneous lidocaine. Subcutaneous and adipose tissue were dissected until the muscle was identified. Muscle tissue was collected, snap-frozen in liquid nitrogen, and stored at -80 °C until analysis.¹⁴

RNA Extraction

Total RNA from calf muscle tissues was isolated using Tri Reagent (Sigma #93289) and chloroform based manual method that yields both mRNA and miRNA. RNA was quantified by measuring absorbance at 260nm using Nanodrop spectrophotometer. The quality of RNA was assessed using Tape station, and in all cases RNA with an RNA integrity number score >6 value was used for mRNA and miRNA-Sequencing (miRNA-Seq).

mRNA Sequencing, Differential Gene Expression, and Biological Pathway Analysis

RNA samples were outsourced to Novogene for mRNA Sequencing performed as per the company's in-house protocol on the Illumina NovaSeq platform (HWI-ST1276) with paired-end 150-bp sequencing strategy; and briefly described here. Original image data file from high-throughput sequencing Illumina platform was transformed to sequenced reads (called raw reads) by CASAVA base recognition (base calling). The mean range of reads per sample were 37 572 436–63 444 164. Raw reads were trimmed to remove reads with adaptor contamination, remove reads when uncertain nucleotides constitute >10% of either read ($n > 10\%$) and remove reads when low quality nucleotides (base quality <5) constitute >50% percent of the read. Quality control of reads demonstrated a Q20(%) score of >97.5 and an error rate <0.03% for all the samples. The trimmed reads were mapped to human genome. Spliced Transcripts Alignment to a Reference software was used to accomplish the mapping. Abundance of transcripts was determined as fragments per kilobase of transcript sequence per millions base pairs. Differential gene expression analysis for 3 sets of comparisons: (1) PAD progression versus non-PAD; (2) PAD no progression versus non-PAD; and (3) PAD progression versus PAD no progression was performed using the DESeq2 R package.²⁰ The false discovery rate was controlled using the Benjamini-Hochberg procedure, and adjusted $P < 0.05$ was considered for statistical significance. Visualization of top significantly upregulated or downregulated genes and their log₂-fold change was performed as volcano plot using ggplot2 package in R program. For further detailed assessment of biological pathways, differentially expressed genes (DEG) with adjusted $P < 0.05$ were used as input in MetaCore pathway analysis (Clarivate Analytics, USA), and significant (nominal $P < 0.05$) biological pathways were identified. Visualization of pathway enrichment analysis was performed as dotplot using ggplot2 package in R program. The RNA-Seq data sets that support the findings of this study are available from the corresponding authors upon reasonable request.

mRNA Real-Time Quantitative PCR

cDNA was generated from 375 ng total RNA using Takara PrimeScript RT reagent Kit with gDNA Eraser (Takara, Cat. No. RR047A) according to the manufacturer's directions. Real-time quantitative PCR (RT-qPCR) was performed in triplicate on a Quantstudio 3 (ThermoFisher Scientific) using GoTaq qPCR Master Mix (Promega, Cat. No. A6001) and primers for *MYBPH* (myosin binding protein H), actin alpha cardiac muscle 1, *CDKN1A* (cyclin dependent kinase inhibitor 1A), phospholipase A2 group IIA, myogenin, *NNMT*

(nicotinamide N-methyltransferase), *HES1* (hairy and enhancer split-1), *HAS2* (hyaluronan synthase 2), *XAF1* (X-linked inhibitor of apoptosis) (XIAP associated factor 1), *ITGA8* (integrin subunit alpha 8), *INHBA* (inhibin subunit beta A) (Invitrogen; primer sequences can be found in Table S1). *L32* (ribosomal protein L32) was used as the reference gene, and relative gene expression was calculated using $2^{-\Delta\Delta CT}$ from the non-PAD group.

miRNA RT-qPCR

cDNA was generated from 50 ng of total RNA using miRCURY LNA RT Kit (Qiagen, Cat. No. 339340) according to the manufacturer's directions. RT-qPCR was performed in triplicate on a Quantstudio 3 (ThermoFisher Scientific) using the miRCURY LNA SYBR Green PCR Kit (Qiagen; Cat. No. 339345) and miRCURY miRNA assay primers for miR-503-5p, miR-223-3p, miR-542-3p, miR-450b-5p, miR-135a-5p, miR-130b-3p (Qiagen, see Table S2 for catalog numbers). U6 (RNA, U6 small nuclear 1) was used as the reference gene and relative gene expression was calculated using $2^{-\Delta\Delta CT}$ from the non-PAD group.

Western Blot Analyses

Whole-tissue homogenates of skeletal muscles were prepared by extracting tissue protein in extraction buffer (20 mmol/L HEPES, pH 7.4, 2 mmol/L EGTA, 1% Triton X-100, 2% glycerol, 50 mmol/L β -glycerophosphate, 1x Halt-protease, and phosphatase inhibitor cocktail [ThermoFisher Scientific, Waltham, MA; Cat#: 1861280]). Muscle tissue (20–30 mg) was immersed in a precooled vial filled with zirconium beads (\varnothing 3 mm) and extraction buffer (1:20 w/v), placed in a BeadBug homogenizer (homogenizer and beads from Benchmark Scientific, Sayreville, NJ), and homogenized 5 times at setting 4000 for 30 seconds each, with intermittent cooling for 1 minute on ice. Subsequently, the cleared homogenate was sonicated 10 times for \approx 3 seconds, followed by centrifugation at 10 000g for 10 minutes at 4 °C. Total protein content of the resulting supernatant was determined via Bradford colorimetric assay. Protein content of selected targets was semiquantified by traditional Western blot as described previously.²¹ Briefly, samples were diluted in Laemmli sample buffer (Bio-Rad, Hercules, CA; Cat#161–0747) supplemented with β -mercaptoethanol, and proteins denatured at 95 °C for 5 minutes. A total of 50 μ g protein was separated on a polyacrylamide gel (Bio-Rad), transferred onto nitrocellulose membranes (Bio-Rad), and blocked in Tris-buffered saline with Tween 20 and 5% fat-free milk. The following commercially available primary antibodies were used: MYBPH (ThermoFisher Scientific, Cat# MA5-26185; 1:4000), myogenin (R&D Systems, Minneapolis, MN, Cat# MAB66861; 1:1000), CDKN1A (p21) (Cell Signaling, Danvers, MA, Cat# 2947; 1:1000),

HES1 (OriGene, Rockville, MD, Cat# TA500114; 1:1000). Secondary antibodies applied were HRP-conjugated anti-mouse or anti-rabbit IgG (Cell Signaling; anti-mouse IgG #7076, anti-rabbit IgG #7074; both 1:5000). Protein bands were detected with SuperSignal West Femto Maximum Sensitivity Substrate (ThermoFisher Scientific) using a ChemiDoc XRS imager (Bio-Rad), and target bands were quantified using the Image Lab 6.0 software (Bio-Rad). The spot density of each band was normalized to the total protein amount loaded in the same lane, as determined by the densitometric analysis of the corresponding Ponceau S-stained membranes.^{22,23}

Immunohistochemistry and Gastrocnemius Muscle Fiber Type Assessment

Immunohistochemical determination of gastrocnemius muscle fiber types and muscle fiber size was carried out as previously described.²⁴ Briefly, fresh frozen muscle biopsies were sectioned at 7 μm in a cryostat, placed onto charged slides (Fisher Scientific, Waltham, MA) and allowed to dry at room temperature for 1 hour. Slides were then washed with PBS, followed by overnight incubation with primary antibody at 4 °C. For detection of fiber borders rabbit anti-laminin (L9393; Sigma-Aldrich, St. Louis, MO) was used in conjunction with the following isoform-specific MyHC (myosin heavy chain) antibodies all from Developmental Studies Hybridoma Bank (Iowa City, IA): Type 1 MyHC (BA.D5; IgG2b), Type 2a MyHC (SC.71; IgG1) and Type 2x MyHC (6H1; IgM). Following overnight incubations, sections were washed 3 times with PBS and incubated for 1 hour with the following secondary antibodies: anti-rabbit IgG H+L AMCA (C1-1000; Vector Laboratories, Burlingame, CA), anti-mouse IgG2b AlexaFluor 647 (A21242, ThermoFisher Scientific, Grand Island, NY), anti-mouse IgG1 AlexaFluor 488 (A21121) and anti-mouse IgM AlexaFluor 555 (A21426). Sections were washed with PBS and cover-slipped with Vectashield (H-1000; Vector Laboratories). Digital images of entire muscle biopsy cross-sections were acquired at 200 \times magnification using an AxioImager M1 fluorescence microscope (Carl Zeiss, Oberkochen, Germany). Muscle fiber type distribution and fiber size were determined using our automated image quantification platform, MyoVision.²⁵ Analysis of satellite cell abundance was performed as follows. Sections were fixed for 3 minutes in -20 °C acetone, washed with PBS, peroxidase quenched using 3% hydrogen peroxide for 8 minutes, washed and blocked for 1 hour in 2.5% NHS (S-2012-50; Vector Laboratories). Sections were incubated overnight with anti-paired box 7 to identify satellite cells (Pax7-c; Developmental Studies Hybridoma Bank). Following PBS washes, biotinylated anti-mouse

IgG1 (115-065-205; Jackson ImmunoResearch Laboratories, West Grove, PA) was applied for 90 minutes, and sections were washed and incubated for 1 hour with streptavidin horseradish peroxidase (S911; ThermoFisher). Superboost tyramide signal amplification AlexaFluor 594 was used for fluorescent labeling and visualization of anti-paired box 7 (B40957; ThermoFisher). Anti-laminin primary antibody was added followed by anti-rabbit AlexaFluor 488 (A11034) to visualize and quantify muscle fibers. Sections were washed, incubated for 10 minutes with DAPI (D1306; ThermoFisher) to label nuclei and cover slipped. Whole cross-section images were acquired with a 20 \times objective, satellite cells were identified as anti-paired box 7+/DAPI+, and quantification was expressed relative to laminin delineated fiber number.

miRNA-Seq, Differential miRNA Expression, and mRNA-miRNA Interaction

RNA samples were outsourced to Exiqon, Qiagen for miRNA-Seq (1 \times 75 bp sequencing-12M reads per sample). Briefly, miRNA molecule was tagged with a Unique Molecular Index,²⁶ and miRNA sequencing was performed on Illumina platform. Following sequencing and trimming, unique molecular index sequence containing reads were mapped to mature miRNA molecule using version of miRbase. Expression levels of each miRNA in a sample were measured as tags per million mapped reads and differential expression of miRNA among groups was performed using the EdgeR statistical software package.²⁷ For normalization, the trimmed mean of M-values method based on log-fold and absolute gene-wise changes in expression levels between samples (trimmed mean of M-values normalization) was used, and miRNA identified at adjusted $P < 0.05$ was considered significant. Differentially expressed miRNA and mRNA (adjusted $P < 0.05$) were used to obtain miRNA-mRNA interactions according to ingenuity pathways analysis microRNA Target Filter tool (ingenuity pathways analysis winter release December 2020). Different miRNA target prediction programs (TargetScan, miRecords, Ingenuity Knowledge Base, and TarBase) filtered our miRNA-mRNA pairings.²⁸ Confidence filter was used by selecting both experimentally observed and predicted target correlations. Targets were selected that were both predicted and experimentally observed. Visualization of miRNA-mRNA interactions was performed as circus plot using circlize package in R program. The miRNA-Seq data sets that support the findings of this study are available from the corresponding authors upon reasonable request.

Statistical Analysis

Baseline characteristics of participants with and without PAD were summarized as means and SDs for

continuous variables and as frequencies and percentages for categorical variables. T-tests were used to compare continuous characteristics, and Chi-square tests and Fisher exact test were used to compare categorical characteristics of participants with and without PAD, when appropriate. Fiber type-specific fiber size differences between patients with PAD with progression or patients with PAD without progression and those with non-PAD and differences in the number of fibers falling within specified fiber size ranges (relative frequency) were determined using a mixed-effects model; in this model, group was the fixed effect, and individual subject was the random effect using the Geisser–Greenhouse correction because of unequal sample sizes. Because of the small sample sizes, adjustment for multiple comparisons was not performed. Analyses were performed using SAS version 9.4 (Cary, NC).

RESULTS

Differential Gene Expression and Pathway Analysis

Participants' clinical characteristics and medications are listed in Table 1. The number of DEG for 3 sets of comparisons: (1) PAD progression versus non-PAD;

(2) PAD no progression versus non-PAD; and (3) PAD progression versus PAD no progression is listed in Figure 1A (*adjusted P value*<0.05; *log2FC*>1), and gene names, fold change, and *P* values are shown in Table S3. The top 10 significantly upregulated and downregulated transcripts are shown in Figure 1B. DEG were most abundant in the comparison of PAD progression versus those without PAD. In this comparison, 99 significantly upregulated genes had a log2 fold change above 1 while 59 significantly downregulated genes had a log2 fold change below -1 (Figure 1B). The top 10 significantly upregulated and downregulated genes are shown in Figure 1C. We validated the expression for several of the top differentially expressed transcripts by RT-qPCR, including transcripts involved in cell cycle/senescence (CDKN1A; NNMT), angiogenesis (HES1), and muscle contraction (actin alpha cardiac muscle 1; MYBPH) (Figure S1A). Similarly, we validated a few downregulated transcripts involved in cell adhesion (ITGA8) and apoptosis (XAF1) (Figure S1B). On the protein level, semiquantitative Western blot analysis was performed using commercially available antibodies to 4 of the markers. Consistent with directionality from the RNA-seq and RT-qPCR analyses, we found that MYBPH protein expression increased by 5.2-fold by Western analysis in the PAD progression group

Table 1. Characteristics of Participants With PAD Progression, PAD No Progression, and Non-PAD

Baseline characteristics	PAD progression (n=7)	PAD no progression (n=6)	Non-PAD (n=7)	<i>P</i> value	<i>P</i> trend
Age (y), mean (SD)*	69.12 (7.86)	66.83 (8.47)	67.07 (5.04)	0.8164	0.5928
Women, n (%)	3 (42.86)	3 (50.00)	3 (42.86)	0.9576	1.0000
Black, n (%)	4 (57.14)	4 (66.67)	4 (57.14)	0.9237	1.0000
Ankle brachial index, mean (SD)†	0.64 (0.14)	0.74 (0.06)	1.21 (0.10)	<0.0001	<0.0001
Body mass index (kg/m ²), mean (SD)	31.33 (4.95)	33.19 (8.50)	28.06 (6.55)	0.3944	0.3766
Current smoker, n (%)	2 (28.57)	4 (66.67)	1 (14.29)	0.1292	0.5753
Myocardial infarction, n (%)	0 (0.00)	0 (0.00)	0 (0.00)	NA	NA
Heart failure, n (%)	1 (14.29)	0 (0.00)	0 (0.00)	0.3763	0.2201
Stroke, n (%)	0 (0.00)	0 (0.00)	0 (0.00)	NA	NA
Angina, n (%)	0 (0.00)	0 (0.00)	0 (0.00)	NA	NA
Pulmonary disease, n (%)	2 (28.57)	0 (0.00)	2 (28.57)	0.3425	1.0000
Cancer, n (%)	2 (28.57)	1 (16.67)	1 (14.29)	0.7765	0.5040
Diabetes, n (%)	2 (28.57)	3 (50.00)	0 (0.00)	0.1119	0.2170
Intermittent claudication, n (%)	2 (28.57)	1 (16.67)	0 (0.00)	0.3231	0.1344
Six-min walk distance (meters), mean (SD)	337.48 (75.90)	367.21 (103.81)	497.30 (169.91)	0.0639	0.0257
Medications					
Antiplatelet drugs	3 (42.86)	5 (83.33)	2 (28.57)	0.1290	0.5930
Anticoagulants, including direct oral anticoagulants	0 (0.00)	0 (0.00)	0 (0.00)	NA	NA
Statin medications	6 (85.71)	5 (83.33)	2 (28.57)	0.0431	0.0250
ACE inhibitors/ARB medications	3 (42.86)	4 (66.67)	0 (0.00)	0.0368	0.0928

ACE indicates angiotensin-converting enzyme; ARB, angiotensin receptor blocker; and PAD, peripheral artery disease.

*Age at the time of the biopsy.

†Ankle brachial index of biopsy leg.

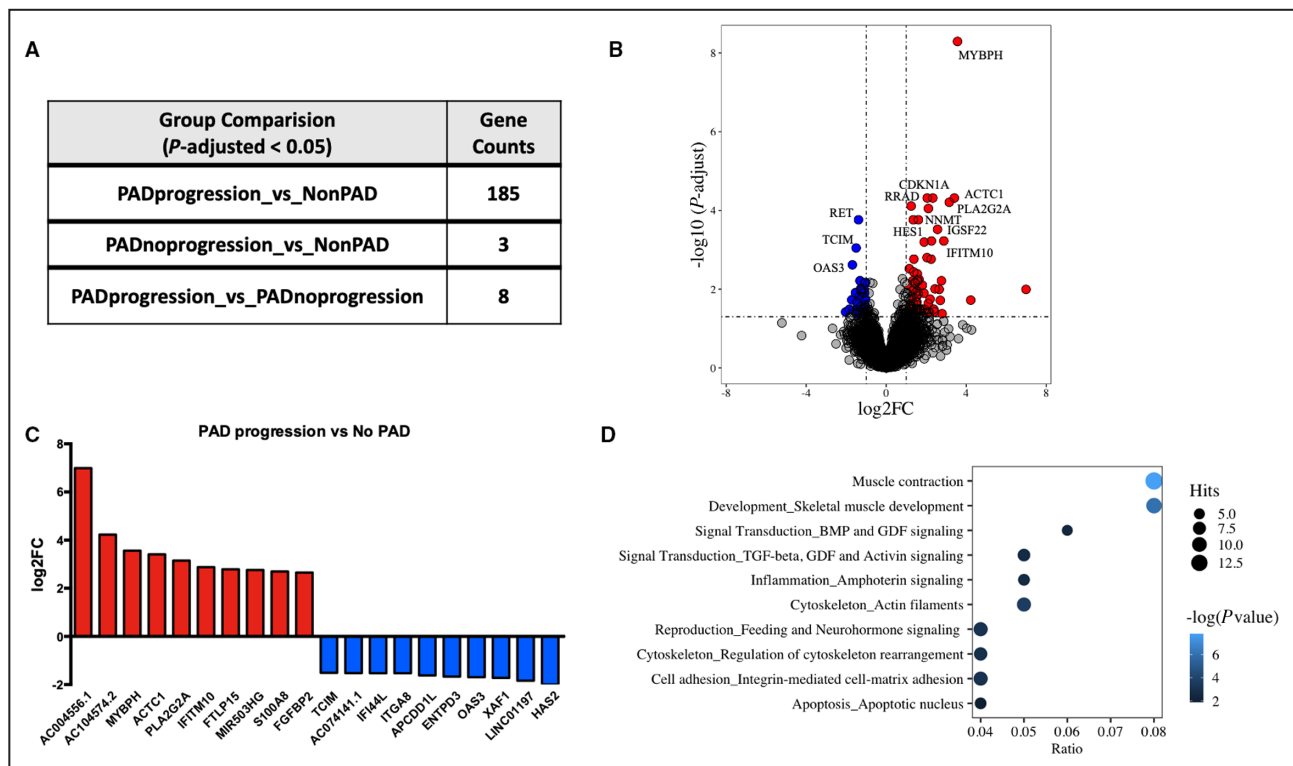


Figure 1. Differentially expressed genes among comparisons of human subjects with PAD progression, PAD no progression, and non-PAD.

A, Gene counts differentially expressed at false discovery rate adjusted at $P < 0.05$. **B**, Names of top 10 significantly upregulated and downregulated genes and their \log_2 fold change. **C**, Volcano plot highlighting differentially expressed genes between PAD progression and non-PAD group at adjusted $P < 0.05$ and \log_2 fold change > 1 ; 99 upregulated genes on upper right quadrant (red dots) and 43 downregulated genes on upper left quadrant (blue dots). **D**, Top 10 significantly enriched pathways associated with differentially expressed genes (nominal $P < 0.05$) between PAD progression and non-PAD group. The size of the dot is ratio of number of genes identified as significantly expressed between PAD progression and non-PAD group and number of genes that constitute that pathway. ACTC1 indicates actin alpha cardiac muscle 1; APCDD1L, adenomatous polyposis coli down-regulated 1-like; BMP, bone morphogenetic protein; ENTDP3, ectonucleoside triphosphate diphosphohydrolase 3; FC, fold change; FGF2, fibroblast growth factor-binding protein 2; FTLP15, ferritin light chain pseudogene 15; GDF, growth/differentiation factor; HAS2, hyaluronan synthase 2; IFI44, interferon induced protein 44; IFITM10, interferon induced transmembrane protein 10; ITGA8, integrin subunit alpha 8; MIR503HG, MIR503 host gene; MYBPH, myosin binding protein H; OAS3, 2'-5'-oligoadenylate synthetase 3; PAD, peripheral artery disease; PLA2G2A, phospholipase A2 group II A; RET, ret proto-oncogene; S100 calcium binding protein A8; TCIM, transcriptional and immune response regulator; TGF, transforming growth factor; and XAF1, XIAP associated factor 1.

compared with the non-PAD control group (Figure S1C), whereas we did not detect discernable trends across the groups for myogenin, or observed weak bands for p21 and HES1 (data not shown). All DEG were annotated for their association with known pathways to understand their biological function. The top 5 significant cellular pathways that were associated with these DEG in people with PAD progression were muscle contraction, skeletal muscle development, bone morphogenetic protein/transforming growth factor-beta (TGF β) and growth/differentiation factor (GDF) signaling, inflammation, and cytoskeleton/actin filaments (Figure 1D). Visualization of gene networks of the "muscle contraction" and "skeletal muscle development" pathways are shown in Figure 2, and those representing "inflammation signaling" and "TGF β , GDF, and actinin signaling" are shown in Figure S2. The

description of significant pathways and the genes involved are listed in Table S4. The number of DEG with adjusted P value < 0.05 was not sufficient to perform pathway analysis for PAD without progression versus non-PAD and PAD progression versus PAD without progression (Figure 1A).

Subjects With PAD With Functional Decline (PAD Progression) Have Smaller Type 2a Gastrocnemius Muscle Fibers

Using immunohistochemistry to identify muscle fiber borders and myosin heavy chain expression, we analyzed both fiber type distribution (data not shown) and fiber type-specific muscle fiber size in gastrocnemius biopsies from patients with PAD with progression and without progression, compared with subjects without

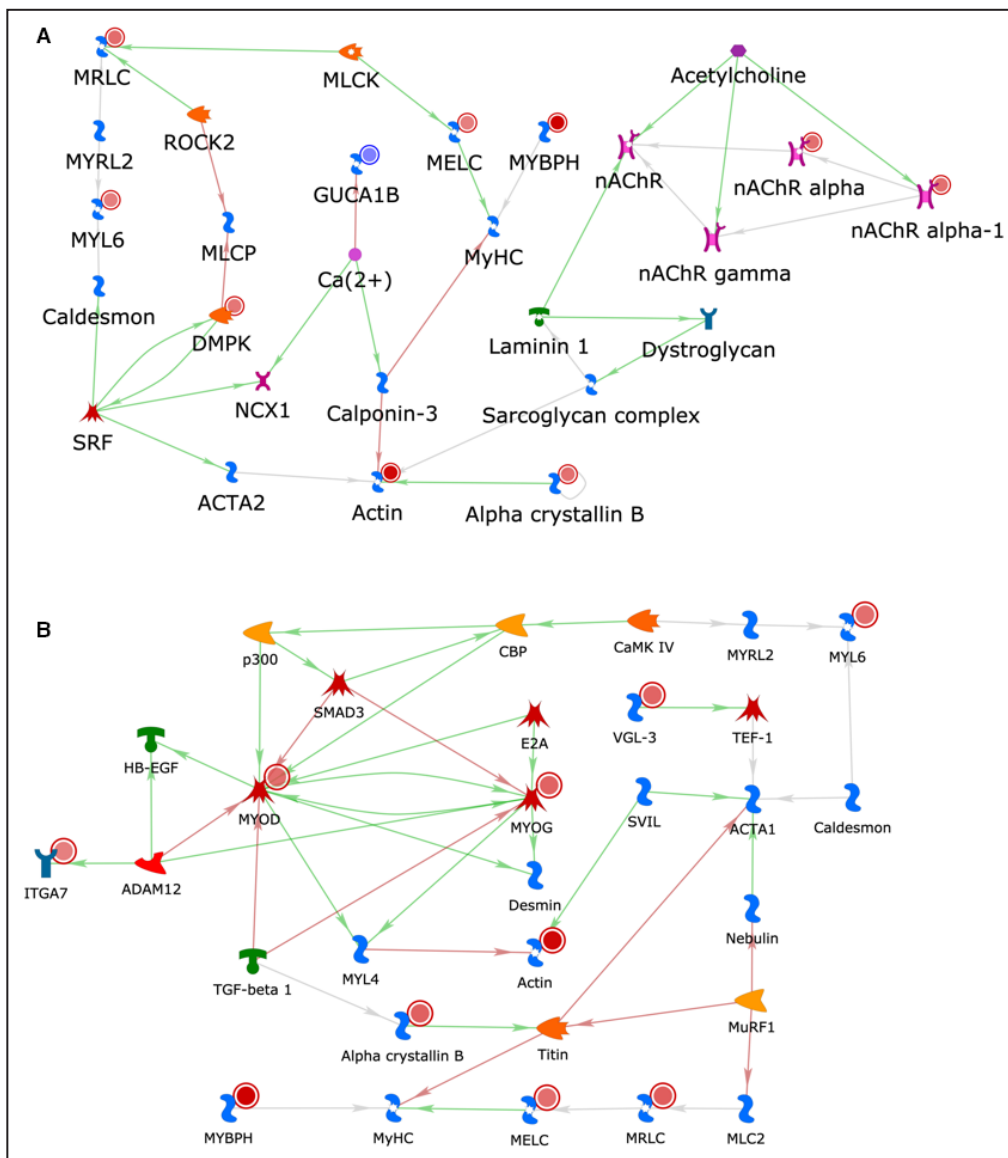


Figure 2. Visualization of gene networks of the “muscle contraction” (A) and “skeletal muscle development” (B) pathways. Blue targets indicate downregulation; red targets indicate upregulation. MYBPH indicates myosin binding protein H.

PAD (non-PAD) (Figure 3). We did not observe significant differences in the frequency of Type 1, Type 2a, or hybrid Type 2a/x muscle fibers among any of these groups (Figure S3A). Similarly, the average muscle fiber size, measured by cross-sectional area, did not differ among groups (Figure S3B). Upon further assessment of fiber size by fiber type, we observed smaller Type 2a fibers within muscle biopsies from patients with PAD with progression compared with both patients with PAD without progression and compared with participants without PAD, though this difference was not significant (Figure 3A). To examine potential differences more closely in the size of Type 2a fibers, we identified the relative frequency of Type 2a fibers (% of total) within

specified ranges based on fiber size: 0–1499, 1500–2999, 3000–4499, and 4500–5999 μm^2 . Comparing among groups, we noted a significant increase in the relative frequency of Type 2a fibers within the smallest size range (0–1499 μm^2) in muscles from patients with PAD with progression (Figure 3B). However, this association was attenuated after adjusting for age ($P=0.0675$). Representative images of fiber type and size from each group are shown in Figure 3C and highlight the presence of small Type 2a fibers in muscles from patients with PAD with progression (white arrows). We also examined satellite cell content (Figure S3C) and macrophage populations (Figure S3D through S3F) but found no significant differences between any group.

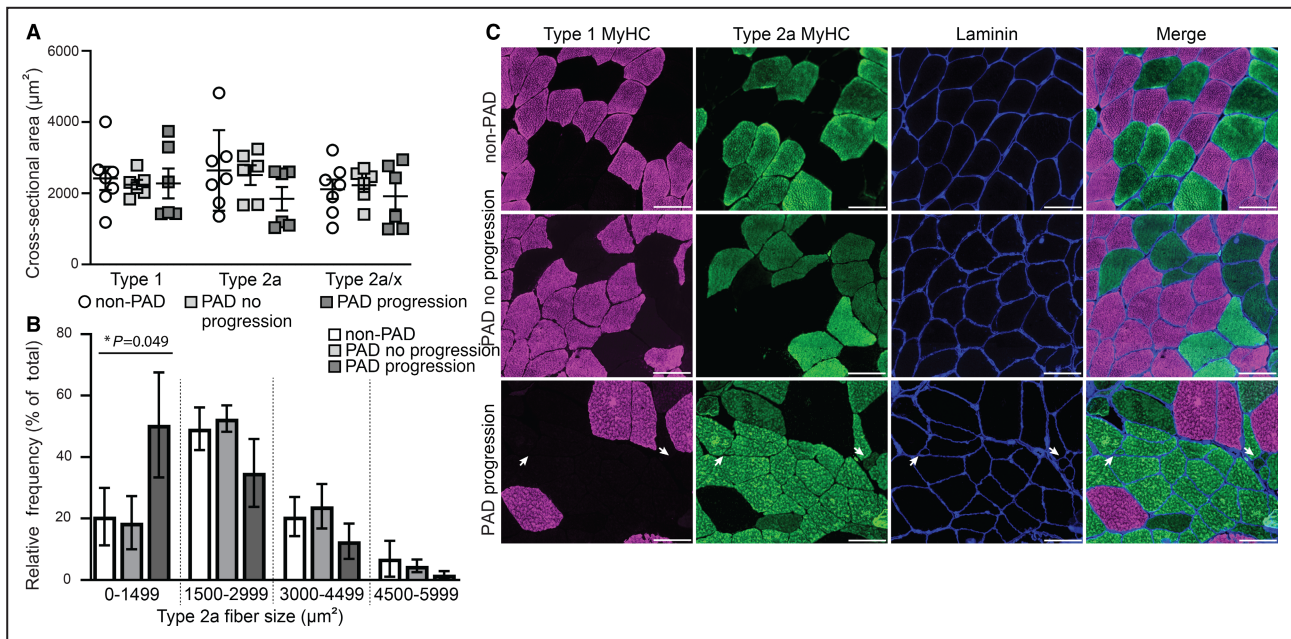


Figure 3. Smaller Type 2a fiber size in gastrocnemius muscle from subjects with PAD with functional decline (PAD progression).

A, Average fiber size (cross-sectional area) stratified by fiber type within subjects without PAD (non-PAD; $n=7$), subjects with PAD without functional decline (PAD no progression; $n=6$), and subjects with PAD and functional decline (PAD progression; $n=6$). Data expressed as mean \pm SEM. **B**, Relative frequency distribution of Type 2a muscle fiber size. Each bar represents the percent of total fibers within the specified fiber size bin (1500- μm width). Note, a greater number of small Type 2a fibers (0–1499 μm^2) within gastrocnemius muscles from the PAD progression group. A mixed effects model was used to determine differences among groups (P value); however, multiple comparisons were not performed because of the small sample sizes. A linear mixed-effects model was used to determine significant differences in cross-sectional area and relative frequency within Type 2a fiber size ranges between non-PAD and PAD progression (0–1499, $P=0.031$). **C**, Representative images of immunohistochemistry depicting fibers expressing Type 1 MyHC (myosin heavy chain, pink), Type 2a MyHC (green) and fiber borders (laminin, blue) from the gastrocnemius muscle of non-PAD (top), PAD no progression (middle) or PAD progression (bottom). White arrows point to several small Type 2a fibers. MyHC indicates myosin heavy chain; and PAD, peripheral artery disease. Scale bar=100 μm .

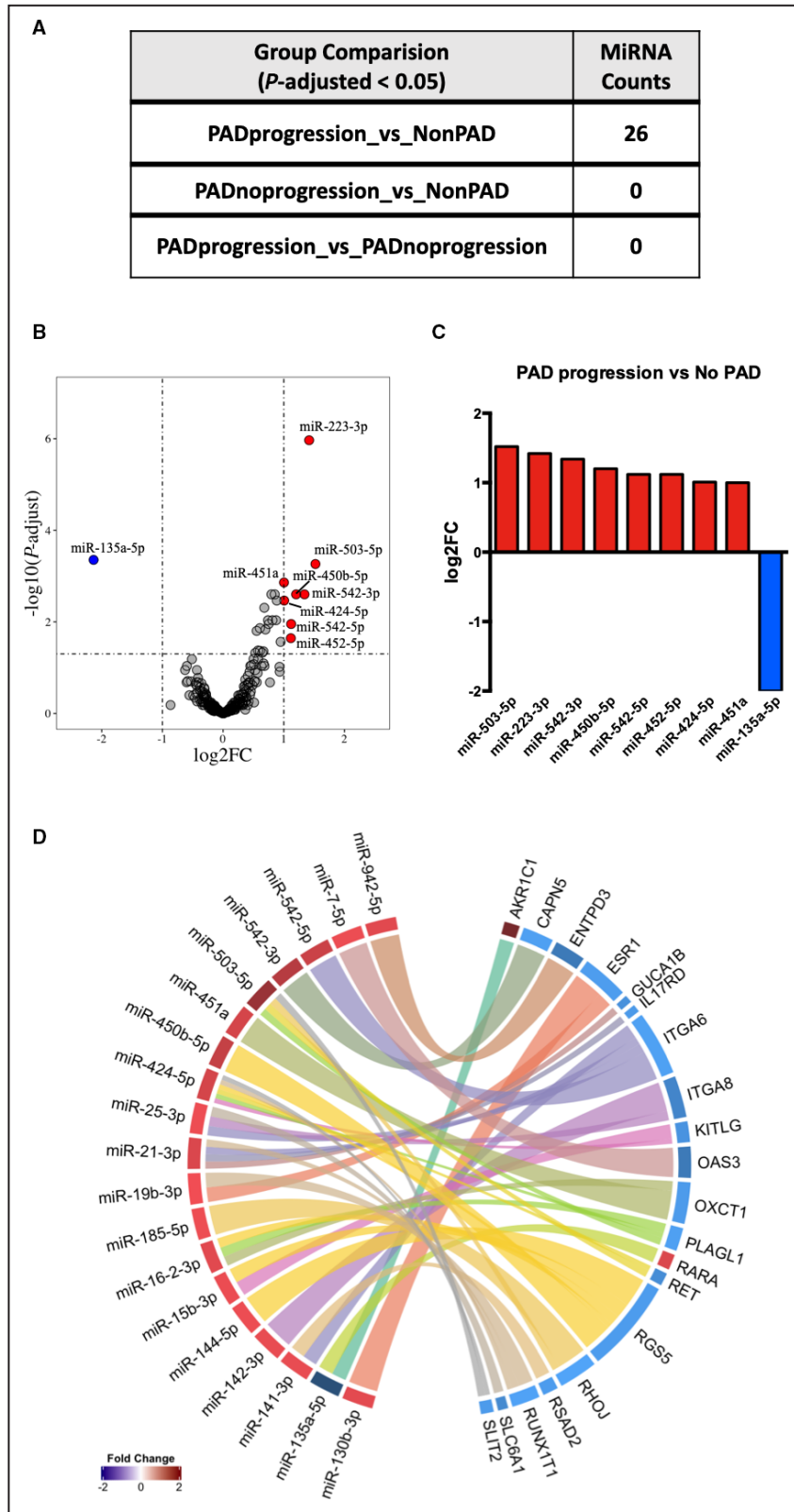
Differentially Expressed miRNA and miRNA-mRNA Interactions

Identification of miRNAs and their associated target genes may provide additional insights into biological pathways relevant to PAD. miRNAs that were significantly differentially expressed (adjusted P value <0.05) were assessed across the 3 groups (Figure 4A). Differential expression analysis showed 25 miRNAs upregulated and 1 miRNA downregulated in PAD progression compared with the non-PAD group (Figure 4B and Table S5). Differentially expressed miRNAs in PAD progression compared with non-PAD group with $\log_2\text{FC}>1$ are shown in Figure 4C. We validated the expression for several of the top differentially expressed miRNA transcripts by RT-qPCR (Figure S4). Targets of the significantly expressed miRNAs (adjusted P value <0.05) were identified from the significantly expressed genes (adjusted P value <0.05) in PAD progression compared with non-PAD group (Figure S5). As miRNA negatively regulates mRNA expression, opposite expression pairing between miRNA and mRNA transcripts was implemented to further analysis. Analysis of miRNA-mRNA

interactions identified 39 interactions. According to the phenomenon of cooperative gene regulation by miRNA pairs, which facilitates a more effective target repression of mRNA transcripts, our results also showed that 1 miRNA may regulate many genes, while 1 gene may be targeted by several miRNAs. Specifically, 18 differentially expressed miRNAs were paired with 20 mRNA targets, including several targets involved in integrin signaling (ITGA6, ITGA8), angiogenesis (Ras homolog family member J), and inflammation (interleukin 17 receptor D) (Figure 4D, Figure S5, and Table S6).

DISCUSSION

Among the comparisons addressed in this study, we found substantial gene expression differences between participants who experienced PAD progression, defined as significant decline in 6-minute walk over 6-month follow-up, compared with participants free of PAD. Enrichment analysis of this set of differentially expressed transcripts indicated a dysregulation of pathways in the PAD progression group compared with healthy controls



related to: (1) skeletal muscle contraction or development; (2) TGF- β , GDF, and activin signaling; and (3) inflammation. Further analysis of the top 10 dysregulated genes revealed transcripts associated not only with

skeletal muscle contraction but also cellular senescence and notch signaling. These findings suggest that while maladaptive pathways are enriched, myogenesis may be activated in people with PAD who experience

Figure 4. Differentially expressed miRNAs among comparisons of human subjects with PAD, PAD no progression, and non-PAD. **A**, miRNA counts differentially expressed at statistical significance of $P < 0.05$ and \log_2 -fold change > 1 . **B**, Volcano plot representing upregulated microRNAs (miRNAs) (8) in upper right quadrant (red dots) and downregulated miRNA (1) in upper left quadrant (blue dot) between PAD progression and non-PAD group. **C**, Top significantly upregulated and downregulated miRNAs and their \log_2 -fold change. **D**, Significantly enriched interactions of miRNA and gene targets that are differentially expressed between PAD progression and non-PAD groups. ENTPD3 indicates ectonucleoside triphosphate diphosphohydrolase 3; FC, fold change; ITGA8, integrin subunit alpha 8; miR, microRNA; miRNA, microRNA; OAS3, 2'-5'-oligoadenylate synthetase 3; RET, ret proto-oncogene; PAD, peripheral artery disease; and XAF1, XIAP associated factor 1.

worsening of 6-minute walk. These changes may represent a compensatory response that is associated with greater severity of disease. However, further study to confirm and extend these findings is needed.

Enrichment of both “TGF- β , GDF, activin signaling” and “inflammation” pathways in the PAD progression group also highlights important roles for key transcripts from these pathways known to be involved in skeletal muscle ischemic injury. For example, the proinflammatory activator protein 1 transcription factor complex is common to both pathways and represents a key downstream mediator of MAPK (mitogen-activated protein kinase) signaling that is increased in response to ischemic injury^{29,30} and promotes skeletal muscle angiogenesis. The activator protein 1 homodimer, Jun D Proto-Oncogene, is enriched in the “TGF- β , GDF, and activin signaling” pathway and activates MMP-2 (matrix metalloproteinase-2). Deficiency of MMP-2 impaired blood flow recovery and triggered limb gangrene after hindlimb ischemia in mice,³¹ raising the possibility that its overexpression may be linked to compensatory vessel remodeling in patients with PAD progression. Finally, calgranulin A (known as S100A8 [S100 calcium binding protein A8]) is also enriched in the “TGF- β , GDF, and activin signaling” pathway and heterodimerizes with S100A9 (S100 calcium binding protein A9) to form calprotectin, an acute phase reactant released from skeletal muscle during exercise.³² Impaired vascular endothelial growth factor receptor 1-S100A8/S100A9 signaling induced an M1-like macrophage phenotype that inhibited ischemic skeletal muscle angiogenesis.³³ S100A8/S100A9 is also associated with increased neutrophil presence and activity, independent of macrophages.²¹ Interestingly, use of neutrophil lymphocyte ratio had been used as a predictor of major amputation and/or mortality in critical limb ischemia.³⁴ Collectively, these findings suggest that gastrocnemius muscles of subjects in the PAD progression group exhibit compensatory signaling pathways enriched for transcripts that are not sufficient to overcome pathologic changes and are insufficient to promote skeletal muscle angiogenesis or improve walking ability.

Whole transcriptome profiling identifies differences in expression of genes and miRNAs in health and disease and also reveal how these differences in expression may inform activation or repression of specific biological pathways. This study sought to identify differences in gene and miRNA expression, as well as

predicted biological pathways among human subjects with PAD progression, PAD no progression, and non-PAD. PAD progression was considered for subjects with PAD who had a meaningful decline by > 25 meters in 6-minute walking distance on 6-month follow-up.³⁵ Decline in walking performance was selected as a criterion for categorizing participants in PAD progression and PAD no progression because decline in functional performance in subjects with PAD predicted later loss in mobility and mortality.^{36,37} Major differences in gene expression between subjects with PAD who had significant decline in walking performance and subjects with non-PAD were enriched for transcripts related to skeletal muscle biology. Among the top 10 significantly upregulated expressed genes between PAD progression and subjects with non-PAD were transcripts associated with skeletal muscle contraction or function (MYBPH, actin alpha cardiac muscle 1, myogenin), cellular senescence (CDKN1A, NNMT), and Notch signaling (Hes1). For example, among the skeletal muscle enriched transcripts include MYBPH, a structural constituent of muscle binds to myosin and helps with muscle contraction; actin alpha cardiac muscle 1, a developmental component of the skeletal muscle contractile apparatus; and myogenin, a muscle-specific transcription factor that induces myogenic differentiation. Along with the above discussed genes, other significantly (with false discovery rate adjusted P value) upregulated genes including *MyHC*, myosin light chain 5, myosin light chain 6, myogenic differentiation 1, troponin C, glycolytic cell derived neurotrophic factor, filamin B, are nearly all related to processes of muscle contraction and muscle tissue development. Indeed, abnormalities in structural proteins, such as actin, myosin, and intermediate filaments, related to the contractibility of skeletal muscle have been previously associated with PAD.^{38,39}

Muscle fiber perturbations have been reported within the gastrocnemius muscle of patients with PAD, and oxidative damage has been proposed to contribute to PAD myopathy.^{1,40–42} Preferential oxidative damage to Type 2 muscle fibers and reductions in Type 2 fiber size were observed in patients with PAD gastrocnemius muscles and were more apparent in end-stage disease.^{1,43–45} Here, we report a higher number of small ($< 1499 \mu\text{m}^2$) Type 2a fibers in the gastrocnemius muscle of patients with PAD with progression (Figure 3), consistent with previous findings.^{1,43–45}

As discussed above, MYBPH protein is involved in myofilament assembly and muscle contraction, and previous reports have associated MYBPH primarily with fast (Type 2) muscle fibers.^{46,47} Interestingly, MYBPH is reportedly high in muscles from individuals with the neurodegenerative disease amyotrophic lateral sclerosis (ALS) and is postulated to cause dysregulation in actin-myosin interaction.^{48,49} Pathogenesis in ALS has been associated with increased oxidative stress within muscles,⁵⁰ and recent mouse models of ALS suggest muscle atrophy may precede and possibly contribute to neuromuscular junction alterations.^{51–53} Type 2 fiber atrophy in PAD gastrocnemius muscles is associated with increases in angular fibers, indicative of denervation,⁴⁵ and the denervation marker neural cell adhesion molecular has been reported within Type 2 fibers from patients with PAD calf muscles.⁵⁴ Together, these findings underscore alterations in the contractile apparatus in muscle from patients with PAD with progression that may be preferential for Type 2 fibers and may precede denervation and fiber loss. On the other hand, it is worth noting that Hiatt et al observed improvement in PAD patients' walking performance, with treadmill training concomitant with increases in markers of denervated fibers, suggesting that this may be an adaptation to PAD.⁵⁵

In addition to MYBPH, expression of the LIM domain kinase 1 (*LIMK1*) gene was also increased in muscle from patients with PAD with progression compared with non-PAD muscle (Table S3). LIMK1 is involved in regulation of the actin cytoskeleton. Phosphorylation of LIMK1 inhibits actin depolymerization through inactivation of cofilin, resulting in actin filament stabilization.^{56,57} Interestingly, MYBPH may inhibit the phosphorylation of LIM kinases through interaction with Rho-associated coiled-coil containing protein kinases, and muscles from patients with ALS with high levels of MYBPH also accumulated nonphosphorylated LIMK1, which may underlie disruption of actin-myosin interactions.⁴⁸ Our findings show higher expression of both MYBPH and LIMK1 genes within gastrocnemius muscles of patients with PAD with progression, suggesting destabilization of actin may be taking place within these muscles. Collectively, smaller Type 2a fibers, coupled with increases in MYBPH and LIMK1 in gastrocnemius muscles from patients with PAD with progression, highlight a potentially novel pathway whereby destabilization of the contractile apparatus may underlie reductions in Type 2a fiber size and may be an early step toward fiber loss and progressive mobility decline. These pathogenic alterations may be subsequent to oxidative damage, preferentially affecting Type 2 fibers and ultimately leading to fiber denervation and mobility loss. Further study is needed to test these hypotheses.

The increased expression of CDKN1A and NNMT transcripts in subjects with PAD progression compared with non-PAD is consistent with

emerging studies linking advanced PAD to dysregulated pathways involved in accelerated cellular senescence.^{26,58,59} CDKN1A, also known as p21 protein, is a potent cyclin-dependent kinase inhibitor that regulates cell cycle progression and is a marker of cellular senescence. Silencing of CDKN1A expression in skeletal muscle ischemic injury models in mice improved capillary density and tissue perfusion.^{60,61} Similarly, NNMT, a cytosolic enzyme overexpressed with aging, controls the expression of nicotinamide molecules required for nicotinamide adenine dinucleotide, a key age-related regulator of metabolism and mitochondrial function in skeletal muscles.⁶² Collectively, expression of these markers raises the possibility that cellular senescence may be deleterious in the PAD progression group.

Skeletal muscles of subjects in the PAD progression group also exhibited increased expression of Hes1, a well-known downstream transcription factor in the Notch signaling pathway linked to impaired angiogenic responses.⁶³ For example, deficiency of Hes1 leads to defective endothelial cell invasion, proliferation, and tube formation in vitro and reduced neovascularization following hindlimb ischemia in mice.⁶⁴ Inhibition of the Hes1 upstream Notch ligand Delta-like 4 also impaired sprouting angiogenesis and proper reparative angiogenesis in skeletal muscles following hindlimb ischemia.⁶⁵ Finally, deficiency of the Notch receptor Notch1 specifically in endothelial cells impaired angiogenesis following ischemic injury in adductor muscles.⁶⁶ Collectively, these pathobiological correlative findings of the Notch signaling pathway raise the possibility that increased expression of Hes1 in the PAD progression group may impede appropriate endothelial sprouting and reparative angiogenesis in gastrocnemius muscles of these patients. Alternatively, increased Hes1 observed in the muscles could be indicative of muscle repair. For example, Hes1 controls the proliferation and activation of muscle stem cells in regenerating muscles.⁶⁷ Furthermore, Hes1 also drives the oscillatory expression of MyoD in muscle stem cells, which we also observed in gastrocnemius muscles of the PAD progression group.

Few genes differed significantly (with false discovery rate adjusted *P* value <0.05) in participants without PAD progression compared with participants without PAD. However, among the above-mentioned genes related to muscle contraction and skeletal muscle development, several were significantly upregulated, with nominal *P* value in the PAD no progression group compared with non-PAD group (Table S3). Moreover, the process of muscle contraction was represented by the topmost significant pathway (false discovery rate adjusted *P* value of 2.64E-05) in the PAD no progression compared with the non-PAD group (Table S4). Taken together, these results suggest that the process of muscle contraction may be upregulated in subjects with PAD, irrespective of stages of disease

progression; however, this process was more stimulated in subjects with progression of disease compared with nonprogressors and highlights a possible pathway associated with mobility loss. Future studies will be required to confirm these findings and assess precise stage-specific roles.

miRNA-Seq revealed significant differences in the expression of 26 miRNAs in patients with PAD progression compared with participants with non-PAD. miR-451a was observed as the most frequently expressed miRNA in muscle and was upregulated by 2-fold in the PAD progression group compared with non-PAD. In the mouse myoblast cell line C2C12, overexpression of miR-451a inhibited myogenic differentiation, suggesting an inhibitory role of this miRNA in myogenesis.⁶⁸ Using a combination of miRNA target prediction algorithms (Figure 4D), data reported here showed that miR-451a targets 3-oxoacid CoA-transferase (OXCT1), an enzyme involved in mitochondrial ketone bodies uptake and oxidation in skeletal muscle. OXCT1 expression is regulated by the coactivator peroxisome proliferator-activated receptor gamma coactivator 1-alpha, a coactivator implicated in angiogenesis and atrophy in skeletal muscles, and was significantly induced in skeletal muscles of human subjects undergoing exercise training compared with sedentary controls.⁶⁹ SLIT2 (slit guidance ligand 2), a member of the secreted Slit family involved in vascular remodeling, is a predicted target of miR-424-5p (Figure S5). Slit2 overexpression in a mouse model decreases vascular endothelial growth factor receptor 2-mediated vascular permeability, blood perfusion, and capillary enlargement in the limb.⁷⁰ Given that miR-451a and miR-424-5p are significantly upregulated and their targets OXCT1 and SLIT2 are significantly downregulated in PAD progression compared with non-PAD, it is possible that enhanced expression of miR-451a and miR-424-5p downregulates OXCT1 and SLIT2 expression. Therefore, downregulation of OXCT1 and SLIT2 by miR-451a and miR-424-5p could affect skeletal muscle ketone uptake and catabolism and vascular remodeling. Taken together, these miRNA-mRNA analyses provide new insights in the pathogenesis of PAD that require further study.

Within the few dysregulated miRNAs captured from sequencing, many have been explored in experimental PAD in mice.⁷¹ For example, inhibition of miR-503 improved blood flow recovery after hindlimb ischemia in streptozotocin-induced diabetic mice.⁷² Furthermore, miR-503 expression was elevated in limb muscles of patients with diabetes undergoing lower limb amputation. Similar to miR-503, miR-223 also impairs hindlimb blood flow recovery in murine experimental PAD.⁷³ Conversely, miR-424 found to be induced in endothelial cells by hypoxia, in turn, further promotes proangiogenic response by stabilizing HIF1 α (hypoxia

inducible factor 1-alpha) transcription.⁷⁴ In this regard, miR-210 is known as the master hypoxia-inducible miRNA (hypoxamiR) because it is regulated by HIF1 α . miR-210 is induced in experimental hindlimb ischemia models and associated with muscle damage mediated by mitochondrial oxidative stress.⁷⁵ In a recent study by Ismael et al, miR-210 expression increased in patients with increasing severity of PAD (with intermittent claudication or critical limb ischemia) and negatively correlated with mitochondrial respiration and walking performance.⁷⁶ However, the expression of miR-210 was not found to be modified in our PAD groups compared with non-PAD. Several differences may account for this, including that the study by Ismael et al used a candidate approach by only focusing on a single microRNA, miR-210, as well as likely differences in baseline characteristics and definition of PAD severity across groups. Collectively, these examples of miRNAs involved with experimental limb ischemia inform potential mechanisms of disease in human PAD progression.

This study has limitations. First, the sample size was small. There was little statistical power to detect significant differences in gene and miRNA expression. Findings should be considered exploratory. Second, the study was limited to identification of biological pathways that may differ between PAD (progression and no progression) and non-PAD and whether these pathways are activated or inhibited requires validation. Third, experimental validation of miRNA targets was not performed. Fourth, there was no validation of these findings in an independent data set of participants with and without PAD. Fifth, given the small sample size and the observational nature of these analyses, no causal inferences can be made. Sixth, because participants with PAD have comorbid diseases, it is possible that the declines in 6-minute walk distance were attributable to a factor other than PAD. Seventh, all non-PAD participants were free of diabetes while a few participants with PAD had diabetes; therefore, differences in gene and miRNA expression between participants with PAD and without PAD may be influenced by diabetes. Eighth, participants with PAD were taking a higher percentage of medications such as statins or angiotensin-converting enzyme inhibitors or angiotensin receptor blockers. It is possible that these differences in medication use may have resulted in confounding. However, both statins and angiotensin-converting enzyme inhibitors/angiotensin receptor blockers confer anti-inflammatory, antiproliferative effects in the pathobiology of atherothrombosis. In addition, while clinical studies demonstrate that statins reduced cardiovascular risk and amputation risk in subjects with PAD, randomized clinical trials have not demonstrated a significant effect of statins on improved walking performance or prevention of disability in people with and without PAD.^{77,78} Therefore, it

seems unlikely that these differences in medications would have meaningfully influenced results reported here.

In summary, patients with PAD and functional decline over 6 months exhibited differences in gene and miRNA expression, signaling pathways, and Type 2a muscle fiber size compared with participants with non-PAD. Because some of these differences also emerged in patients with PAD who did not lose walking ability compared with participants without PAD, further study is needed to confirm these findings and determine whether the transcripts may serve as potential biomarkers for diagnosis and staging of disease and whether the identified targets may serve as mediators of the progression of PAD.

ARTICLE INFORMATION

Received July 10, 2021; accepted September 8, 2022.

Affiliations

All India Institute of Medical Sciences, Department of Biophysics, New Delhi, India (S.K.S.); Cardiovascular Division, Department of Medicine, Brigham and Women's Hospital and Harvard Medical School, Boston, MA (D.P.-C., H.S.C., M.W.F.); Department of Physiology, University of Valencia and INCLIVA Biomedical Research Institute, Valencia, Spain (D.P.-C.); Center for Muscle Biology, College of Health Sciences, University of Kentucky, Lexington, KY (K.K., C.A.P.); Department of Preventive Medicine, Northwestern University Feinberg School of Medicine, Chicago, IL (L.L., M.M.M.); Department of Health Research and Policy, Stanford University, Stanford, CA (L.T.); Department of Applied Physiology & Kinesiology, University of Florida, Gainesville, FL (G.D., T.R.); Department of Aging and Geriatric Research, University of Florida, Institute on Aging, Gainesville, FL (K.K.W., B.B., S.E.W., C.L.); Department of Medicine, Northwestern University Feinberg School of Medicine, Chicago, IL (R.L.S., M.M.M.); and Division of Intramural Research, National Institute on Aging, Baltimore, MD (L.F.).

Sources of Funding

This work was supported by the National Institutes of Health (HL115141, HL134849, HL148207, HL148355, HL153356 to M.W.F.; HL122846, HL107510, AG047510, HL126117, to M.M.M.), and the American Heart Association (18SFRN33900144 and 20SFRN35200163 to M.W.F.; 18SFRN33900097 and 18SFRN33900142 to M.M.M.).

Disclosures

Dr McDermott reports research funding from Regeneron and Helixmith and other research support from Mars, ArtAssist, Chromadex, Helixmith, and Regeneron. The remaining authors have no disclosures to report.

Supplemental Material

Tables S1–S6
Figures S1–S5

REFERENCES

- Koutakis P, Weiss DJ, Miserlis D, Shostrom VK, Papoutsis E, Ha DM, Carpenter LA, McComb RD, Casale GP, Pipinos, II. Oxidative damage in the gastrocnemius of patients with peripheral artery disease is myofiber type selective. *Redox Biol*. 2014;2:921–928. doi: [10.1016/j.redox.2014.07.002](https://doi.org/10.1016/j.redox.2014.07.002)
- Weiss DJ, Casale GP, Koutakis P, Nella AA, Swanson SA, Zhu Z, Miserlis D, Johanning JM, Pipinos, II. Oxidative damage and myofiber degeneration in the gastrocnemius of patients with peripheral arterial disease. *J Transl Med*. 2013;11:230.
- Mitchell RG, Duscha BD, Robbins JL, Redfern SI, Chung J, Bensimhon DR, Kraus WE, Hiatt WR, Regensteiner JG, Annex BH. Increased levels of apoptosis in gastrocnemius skeletal muscle in patients with peripheral arterial disease. *Vasc Med*. 2007;12:285–290. doi: [10.1177/1358663X07084858](https://doi.org/10.1177/1358663X07084858)
- Koutakis P, Myers SA, Cluff K, Ha DM, Haynatzki G, McComb RD, Uchida K, Miserlis D, Papoutsis E, Johanning JM, et al. Abnormal myofiber morphology and limb dysfunction in claudication. *J Surg Res*. 2015;196:172–179. doi: [10.1016/j.jss.2015.02.011](https://doi.org/10.1016/j.jss.2015.02.011)
- Pipinos II, Sharov VG, Shepard AD, Anagnostopoulos PV, Katsamouris A, Todor A, Filis KA, Sabbah HN. Abnormal mitochondrial respiration in skeletal muscle in patients with peripheral arterial disease. *J Vasc Surg*. 2003;38:827–832. doi: [10.1016/S0741-5214\(03\)00602-5](https://doi.org/10.1016/S0741-5214(03)00602-5)
- Ryan TE, Yamaguchi DJ, Schmidt CA, Zeczycki TN, Shaikh SR, Brophy P, Green TD, Tarpey MD, Karnekar R, Goldberg EJ, et al. Extensive skeletal muscle cell mitochondriopathy distinguishes critical limb ischemia patients from claudicants. *JCI Insight*. 2018;3:e123235. doi: [10.1172/jci.insight.123235](https://doi.org/10.1172/jci.insight.123235)
- McDermott MM, Hoff F, Ferrucci L, Pearce WH, Guralnik JM, Tian L, Liu K, Schneider JR, Sharma L, Tan J, et al. Lower extremity ischemia, calf skeletal muscle characteristics, and functional impairment in peripheral arterial disease. *J Am Geriatr Soc*. 2007;55:400–406. doi: [10.1111/j.1532-5415.2007.01092.x](https://doi.org/10.1111/j.1532-5415.2007.01092.x)
- McDermott MM. Lower extremity manifestations of peripheral artery disease: the pathophysiologic and functional implications of leg ischemia. *Circ Res*. 2015;116:1540–1550. doi: [10.1161/CIRCRESAHA.114.303517](https://doi.org/10.1161/CIRCRESAHA.114.303517)
- McDermott MM, Ferrucci L, Gonzalez-Freire M, Kosmac K, Leeuwenburgh C, Peterson CA, Saini S, Sufit R. Skeletal muscle pathology in peripheral artery disease: a brief review. *Arterioscler Thromb Vasc Biol*. 2020;40:2577–2585. doi: [10.1161/ATVBAHA.120.313831](https://doi.org/10.1161/ATVBAHA.120.313831)
- Cheng B, Li JY, Li XC, Wang XF, Wang ZJ, Liu J, Deng AP. MiR-323b-5p acts as a novel diagnostic biomarker for critical limb ischemia in type 2 diabetic patients. *Sci Rep*. 2018;8: 15080. doi: [10.1038/s41598-018-33310-4](https://doi.org/10.1038/s41598-018-33310-4)
- Gebert LFR, MacRae IJ. Regulation of microRNA function in animals. *Nat Rev Mol Cell Biol*. 2019;20:21–37. doi: [10.1038/s41580-018-0045-7](https://doi.org/10.1038/s41580-018-0045-7)
- Mendell JT, Olson EN. MicroRNAs in stress signaling and human disease. *Cell*. 2012;148:1172–1187. doi: [10.1016/j.cell.2012.02.005](https://doi.org/10.1016/j.cell.2012.02.005)
- McDermott MM, Leeuwenburgh C, Guralnik JM, Tian L, Sufit R, Zhao L, Criqui MH, Kibbe MR, Stein JH, Lloyd-Jones D. Effect of resveratrol on walking performance in older people with peripheral artery disease: the RESTORE randomized clinical trial. *JAMA Cardiol*. 2017;2:902–907. doi: [10.1001/jamacardio.2017.0538](https://doi.org/10.1001/jamacardio.2017.0538)
- McDermott MM, Criqui MH, Domanchuk K, Ferrucci L, Guralnik JM, Kibbe MR, Kosmac K, Kramer CM, Leeuwenburgh C, Li L. Cocoa to improve walking performance in older people with peripheral artery disease: the COCOA-PAD pilot randomized clinical trial. *Circ Res*. 2020;126:589–599. doi: [10.1161/CIRCRESAHA.119.315600](https://doi.org/10.1161/CIRCRESAHA.119.315600)
- McDermott MM, Spring B, Tian L, Treat-Jacobson D, Ferrucci L, Lloyd-Jones D, Zhao L, Polonsky T, Kibbe MR, Bazzano L, et al. Effect of low-intensity vs high-intensity home-based walking exercise on walk distance in patients with peripheral artery disease: the LITE randomized clinical trial. *JAMA*. 2021;325:1266–1276. doi: [10.1001/jama.2021.2536](https://doi.org/10.1001/jama.2021.2536)
- McDermott MM, Ferrucci L, Tian L, Guralnik JM, Lloyd-Jones D, Kibbe MR, Polonsky TS, Domanchuk K, Stein JH, Zhao L, et al. Effect of granulocyte-macrophage Colony-stimulating factor with or without supervised exercise on walking performance in patients with peripheral artery disease: the PROPEL randomized clinical trial. *JAMA*. 2017;318:2089–2098. doi: [10.1001/jama.2017.17437](https://doi.org/10.1001/jama.2017.17437)
- McDermott MM, Criqui MH, Liu K, Guralnik JM, Greenland P, Martin GJ, Pearce W. Lower ankle/brachial index, as calculated by averaging the dorsalis pedis and posterior tibial arterial pressures, and association with leg functioning in peripheral arterial disease. *J Vasc Surg*. 2000;32:1164–1171. doi: [10.1067/mva.2000.108640](https://doi.org/10.1067/mva.2000.108640)
- McDermott MM, Greenland P, Liu K, Guralnik JM, Celic L, Criqui MH, Chan C, Martin GJ, Schneider J, Pearce WH, et al. The ankle brachial index is associated with leg function and physical activity: the walking and leg circulation study. *Ann Intern Med*. 2002;136:873–883. doi: [10.7326/0003-4819-136-12-200206180-00008](https://doi.org/10.7326/0003-4819-136-12-200206180-00008)
- Shadman R, Criqui MH, Bundens WP, Fronek A, Denenberg JO, Gamst AC, McDermott MM. Subclavian artery stenosis: prevalence, risk factors, and association with cardiovascular diseases. *J Am Coll Cardiol*. 2004;44:618–623. doi: [10.1016/j.jacc.2004.04.044](https://doi.org/10.1016/j.jacc.2004.04.044)
- Haemmig S, Yang D, Sun X, Das D, Ghaffari S, Molinaro R, Chen L, Deng Y, Freeman D, Moullan N, et al. Long noncoding RNA SNHG12 integrates a DNA-PK-mediated DNA damage response and vascular

- senescence. *Sci Transl Med.* 2020;12:eaaw1868. doi: [10.1126/scitranslmed.aaw1868](https://doi.org/10.1126/scitranslmed.aaw1868)
21. Picca A, Saini SK, Mankowski RT, Kamenov G, Anton SD, Manini TM, Buford TW, Wohlgemuth SE, Xiao R, Calvani R, Coelho-Júnior HJ, Landi F, Bernabei R, Hood DA, Marzetti E, Leeuwenburgh C Altered expression of mitoferrin and frataxin, larger labile iron Pool and greater mitochondrial DNA damage in the skeletal muscle of older adults. *Cells.* 2020;9:2579. doi: [10.3390/cells9122579](https://doi.org/10.3390/cells9122579)
 22. Fosang AJ, Colbran RJ. Transparency is the key to quality. *J Biol Chem.* 2015;290:29692–29694. doi: [10.1074/jbc.E115.000002](https://doi.org/10.1074/jbc.E115.000002)
 23. Thacker JS, Yeung DH, Staines WR, Mielke JG. Total protein or high-abundance protein: which offers the best loading control for Western blotting? *Anal Biochem.* 2016;496:76–78. doi: [10.1016/j.ab.2015.11.022](https://doi.org/10.1016/j.ab.2015.11.022)
 24. Murach KA, Dungan CM, Kosmac K, Voigt TB, Tourville TW, Miller MS, Bamman MM, Peterson CA, Toth MJ. Cores of reproducibility in physiology (CORP): fiber typing human skeletal muscle with fluorescent immunohistochemistry. *J Appl Physiol (1985).* 2019;127:1632–1639. doi: [10.1152/jappphysiol.00624.2019](https://doi.org/10.1152/jappphysiol.00624.2019)
 25. Wen Y, Murach KA, Vechetti IJ Jr, Fry CS, Vickery C, Peterson CA, McCarthy JJ, Campbell KS. MyoVision: software for automated high-content analysis of skeletal muscle immunohistochemistry. *J Appl Physiol (1985).* 2018;124:40–51. doi: [10.1152/jappphysiol.00762.2017](https://doi.org/10.1152/jappphysiol.00762.2017)
 26. Katsuomi G, Shimizu I, Yoshida Y, Minamino T. Vascular senescence in cardiovascular and metabolic diseases. *Front Cardiovasc Med.* 2018;5:18. doi: [10.3389/fcvm.2018.00018](https://doi.org/10.3389/fcvm.2018.00018)
 27. Robinson MD, McCarthy DJ, Smyth GK. edgeR: a Bioconductor package for differential expression analysis of digital gene expression data. *Bioinformatics.* 2010;26:139–140. doi: [10.1093/bioinformatics/btp616](https://doi.org/10.1093/bioinformatics/btp616)
 28. Icli B, Wu W, Ozdemir D, Li H, Cheng HS, Haemmig S, Liu X, Giatsidis G, Avci SN, Lee N, et al. MicroRNA-615-5p regulates angiogenesis and tissue repair by targeting AKT/eNOS (protein kinase B/endothelial nitric oxide synthase) signaling in endothelial cells. *Arterioscler Thromb Vasc Biol.* 2019;39:1458–1474. doi: [10.1161/ATVBAHA.119.312726](https://doi.org/10.1161/ATVBAHA.119.312726)
 29. Boerckel JD, Chandrasekharan UM, Waitkus MS, Tillmann EG, Bartlett R, Dicolorio PE. Mitogen-activated protein kinase phosphatase-1 promotes neovascularization and angiogenic gene expression. *Arterioscler Thromb Vasc Biol.* 2014;34:1020–1031. doi: [10.1161/ATVBAHA.114.303403](https://doi.org/10.1161/ATVBAHA.114.303403)
 30. Ramo K, Sugamura K, Craige S, Keaney JF, Davis RJ. Suppression of ischemia in arterial occlusive disease by JNK-promoted native collateral artery development. *Elife.* 2016;5:e18414. doi: [10.7554/eLife.18414](https://doi.org/10.7554/eLife.18414)
 31. Lee JG, Dahi S, Mahimkar R, Tulloch NL, Alfonso-Jaume MA, Lovett DH, Sarkar R. Intronic regulation of matrix metalloproteinase-2 revealed by in vivo transcriptional analysis in ischemia. *Proc Natl Acad Sci USA.* 2005;102:16345–16350. doi: [10.1073/pnas.0508085102](https://doi.org/10.1073/pnas.0508085102)
 32. Mortensen OH, Andersen K, Fischer C, Nielsen AR, Nielsen S, Akerstrom T, Aastrom MB, Borup R, Pedersen BK. Calprotectin is released from human skeletal muscle tissue during exercise. *J Physiol.* 2008;586:3551–3562. doi: [10.1113/jphysiol.2008.153551](https://doi.org/10.1113/jphysiol.2008.153551)
 33. Ganta VC, Choi M, Farber CR, Annex BH. Antiangiogenic VEGF165b regulates macrophage polarization via S100A8/S100A9 in peripheral artery disease. *Circulation.* 2019;139:226–242. doi: [10.1161/CIRCULATIONAHA.118.034165](https://doi.org/10.1161/CIRCULATIONAHA.118.034165)
 34. Bhat TM, Afari ME, Garcia LA. Neutrophil lymphocyte ratio in peripheral vascular disease: a review. *Expert Rev Cardiovasc Ther.* 2016;14:871–875. doi: [10.1586/14779072.2016.1165091](https://doi.org/10.1586/14779072.2016.1165091)
 35. McDermott MM, Tian L, Criqui MH, Ferrucci L, Conte MS, Zhao L, Li L, Sufit R, Polonsky TS, Kibbe MR, et al. Meaningful change in 6-minute walk in people with peripheral artery disease. *J Vasc Surg.* 2021;73:267–276.e1. doi: [10.1016/j.jvs.2020.03.052](https://doi.org/10.1016/j.jvs.2020.03.052)
 36. McDermott MM, Liu K, Ferrucci L, Tian L, Guralnik JM, Liao Y, Criqui MH. Decline in functional performance predicts later increased mobility loss and mortality in peripheral arterial disease. *J Am Coll Cardiol.* 2011;57:962–970. doi: [10.1016/j.jacc.2010.09.053](https://doi.org/10.1016/j.jacc.2010.09.053)
 37. Hammond MM, Tian L, Zhao L, Zhang D, McDermott MM. One-year change in walking performance and subsequent mobility loss and mortality rates in peripheral artery disease: longitudinal data from the WALCS. *J Am Heart Assoc.* 2021;10:e021917. doi: [10.1161/JAHA.121.021917](https://doi.org/10.1161/JAHA.121.021917)
 38. Sjöström M, Angquist KA, Rais O. Intermittent claudication and muscle fiber fine structure: correlation between clinical and morphological data. *Ultrastruct Pathol.* 1980;1:309–326. doi: [10.3109/01913128009141434](https://doi.org/10.3109/01913128009141434)
 39. Koutakis P, Miserlis D, Myers SA, Kim JK, Zhu Z, Papoutsis E, Swanson SA, Haynatzki G, Ha DM, Carpenter LA, et al. Abnormal accumulation of desmin in gastrocnemius myofibers of patients with peripheral artery disease: associations with altered myofiber morphology and density, mitochondrial dysfunction and impaired limb function. *J Histochem Cytochem.* 2015;63:256–269. doi: [10.1369/0022155415569348](https://doi.org/10.1369/0022155415569348)
 40. Koutakis P, Ismaeel A, Farmer P, Purcell S, Smith RS, Eidson JL and Bohannon WT. Oxidative stress and antioxidant treatment in patients with peripheral artery disease. *Physiol Rep.* 2018;6:e13650. doi: [10.14814/phy2.13650](https://doi.org/10.14814/phy2.13650)
 41. Pipinos II, Judge AR, Selsby JT, Zhu Z, Swanson SA, Nella AA, Dodd SL. The myopathy of peripheral arterial occlusive disease: part 2. Oxidative stress, neuropathy, and shift in muscle fiber type. *Vasc Endovascular Surg.* 2008;42:101–112. doi: [10.1177/1538574408315995](https://doi.org/10.1177/1538574408315995)
 42. Pipinos II, Judge AR, Zhu Z, Selsby JT, Swanson SA, Johanning JM, Baxter BT, Lynch TG, Dodd SL. Mitochondrial defects and oxidative damage in patients with peripheral arterial disease. *Free Radic Biol Med.* 2006;41:262–269. doi: [10.1016/j.freeradbiomed.2006.04.003](https://doi.org/10.1016/j.freeradbiomed.2006.04.003)
 43. Clyne CA, Mears H, Weller RO, O'Donnell TF. Calf muscle adaptation to peripheral vascular disease. *Cardiovasc Res.* 1985;19:507–512. doi: [10.1093/cvr/19.8.507](https://doi.org/10.1093/cvr/19.8.507)
 44. McGuigan MR, Bronks R, Newton RU, Sharman MJ, Graham JC, Cody DV, Kraemer WJ. Muscle fiber characteristics in patients with peripheral arterial disease. *Med Sci Sports Exerc.* 2001;33:2016–2021. doi: [10.1097/00005768-200112000-00007](https://doi.org/10.1097/00005768-200112000-00007)
 45. Regensteiner JG, Wolfel EE, Brass EP, Carry MR, Ringel SP, Hargarten ME, Stamm ER, Hiatt WR. Chronic changes in skeletal muscle histology and function in peripheral arterial disease. *Circulation.* 1993;87:413–421. doi: [10.1161/01.CIR.87.2.413](https://doi.org/10.1161/01.CIR.87.2.413)
 46. Bahler M, Eppenberger HM, Wallimann T. Novel thick filament protein of chicken pectoralis muscle: the 86 kd protein. II. Distribution and localization. *J Mol Biol.* 1985;186:393–401. doi: [10.1016/0022-2836\(85\)90113-5](https://doi.org/10.1016/0022-2836(85)90113-5)
 47. Bennett P, Craig R, Starr R, Offer G. The ultrastructural location of C-protein, X-protein and H-protein in rabbit muscle. *J Muscle Res Cell Motil.* 1986;7:550–567. doi: [10.1007/BF01753571](https://doi.org/10.1007/BF01753571)
 48. Conti A, Riva N, Pesca M, Iannaccone S, Cannistraci CV, Corbo M, Previtali SC, Quattrini A, Alessio M. Increased expression of myosin binding protein H in the skeletal muscle of amyotrophic lateral sclerosis patients. *Biochim Biophys Acta.* 2014;1842:99–106. doi: [10.1016/j.bbadis.2013.10.013](https://doi.org/10.1016/j.bbadis.2013.10.013)
 49. Henderson CA, Gomez CG, Novak SM, Mi-Mi L, Gregorio CC. Overview of the muscle cytoskeleton. *Compr Physiol.* 2017;7:891–944.
 50. Barber SC, Mead RJ, Shaw PJ. Oxidative stress in ALS: a mechanism of neurodegeneration and a therapeutic target. *Biochim Biophys Acta.* 2006;1762:1051–1067. doi: [10.1016/j.bbadis.2006.03.008](https://doi.org/10.1016/j.bbadis.2006.03.008)
 51. Dobrowolny G, Aucello M, Musaro A. Muscle atrophy induced by SOD1G93A expression does not involve the activation of caspase in the absence of denervation. *Skelet Muscle.* 2011;1:3. doi: [10.1186/2044-5040-1-3](https://doi.org/10.1186/2044-5040-1-3)
 52. Dobrowolny G, Aucello M, Rizzuto E, Beccafico S, Mammucari C, Boncompagni S, Belia S, Wannenes F, Nicoletti C, Del Prete Z, et al. Skeletal muscle is a primary target of SOD1G93A-mediated toxicity. *Cell Metab.* 2008;8:425–436. doi: [10.1016/j.cmet.2008.09.002](https://doi.org/10.1016/j.cmet.2008.09.002)
 53. Wong M, Martin LJ. Skeletal muscle-restricted expression of human SOD1 causes motor neuron degeneration in transgenic mice. *Hum Mol Genet.* 2010;19:2284–2302. doi: [10.1093/hmg/ddq106](https://doi.org/10.1093/hmg/ddq106)
 54. McDermott MM, Dayanidhi S, Kosmac K, Saini S, Slys J, Leeuwenburgh C, Hartnell L, Sufit R, Ferrucci L. Walking exercise therapy effects on lower extremity skeletal muscle in peripheral artery disease. *Circ Res.* 2021;128:1851–1867. doi: [10.1161/CIRCRESAHA.121.318242](https://doi.org/10.1161/CIRCRESAHA.121.318242)
 55. Hiatt WR, Regensteiner JG, Wolfel EE, Carry MR, Brass EP. Effect of exercise training on skeletal muscle histology and metabolism in peripheral arterial disease. *J Appl Physiol (1985).* 1996;81:780–788. doi: [10.1152/jappl.1996.81.2.780](https://doi.org/10.1152/jappl.1996.81.2.780)
 56. Arber S, Barbayannis FA, Hanser H, Schneider C, Stanyon CA, Bernard O, Caroni P. Regulation of actin dynamics through phosphorylation of cofilin by LIM-kinase. *Nature.* 1998;393:805–809. doi: [10.1038/31729](https://doi.org/10.1038/31729)
 57. Yang N, Higuchi O, Ohashi K, Nagata K, Wada A, Kangawa K, Nishida E, Mizuno K. Cofilin phosphorylation by LIM-kinase 1 and its role in Rac-mediated Actin reorganization. *Nature.* 1998;393:809–812. doi: [10.1038/31735](https://doi.org/10.1038/31735)
 58. Gardner AW, Parker DE, Montgomery PS, Sosnowska D, Casanegra AI, Ungvari Z, Csiszar A, Sonntag WE. Greater endothelial apoptosis and oxidative stress in patients with peripheral artery disease. *Int J Vasc Med.* 2014;2014:160534–160538. doi: [10.1155/2014/160534](https://doi.org/10.1155/2014/160534)

59. Sosinska-Zawierucha P, Mackowiak B, Staniszewski R, Suminska-Jasinska K, Maj M, Krasinski Z, Breborowicz A. Sulodexide slows down the senescence of aortic endothelial cells exposed to serum from patients with peripheral artery diseases. *Cell Physiol Biochem*. 2018;45:2225–2232. doi: [10.1159/000488167](https://doi.org/10.1159/000488167)
60. Shu X, Mao Y, Li Z, Wang W, Chang Y, Liu S, Li XQ. MicroRNA93 regulates angiogenesis in peripheral arterial disease by targeting CDKN1A. *Mol Med Rep*. 2019;19:5195–5202. doi: [10.3892/mmr.2019.10196](https://doi.org/10.3892/mmr.2019.10196)
61. Gogiraju R, Xu X, Bochenek ML, Steinbrecher JH, Lehnart SE, Wenzel P, Kessel M, Zeisberg EM, Dobbstein M, Schafer K. Endothelial p53 deletion improves angiogenesis and prevents cardiac fibrosis and heart failure induced by pressure overload in mice. *J Am Heart Assoc*. 2015;4:e001770. doi: [10.1161/JAHA.115.001770](https://doi.org/10.1161/JAHA.115.001770)
62. Gomes AP, Price NL, Ling AJ, Moslehi JJ, Montgomery MK, Rajman L, White JP, Teodoro JS, Wrann CD, Hubbard BP, et al. Declining NAD(+) induces a pseudohypoxic state disrupting nuclear-mitochondrial communication during aging. *Cell*. 2013;155:1624–1638.
63. Herbert SP, Stainier DY. Molecular control of endothelial cell behaviour during blood vessel morphogenesis. *Nat Rev Mol Cell Biol*. 2011;12:551–564. doi: [10.1038/nrm3176](https://doi.org/10.1038/nrm3176)
64. Jiang H, Cheng XW, Shi GP, Hu L, Inoue A, Yamamura Y, Wu H, Takeshita K, Li X, Huang Z, et al. Cathepsin K-mediated Notch1 activation contributes to neovascularization in response to hypoxia. *Nat Commun*. 2014;5:3838. doi: [10.1038/ncomms4838](https://doi.org/10.1038/ncomms4838)
65. Al Haj Zen A, Oikawa A, Bazan-Peregrino M, Meloni M, Emanuelli C, Madeddu P. Inhibition of delta-like-4-mediated signaling impairs reparative angiogenesis after ischemia. *Circ Res*. 2010;107:283–293. doi: [10.1161/CIRCRESAHA.110.221663](https://doi.org/10.1161/CIRCRESAHA.110.221663)
66. Takeshita K, Satoh M, Li M, Silver M, Limbourg FP, Mukai Y, Rikitake Y, Radtke F, Gridley T, Losordo DW, Liao JK. Critical role of endothelial Notch1 signaling in postnatal angiogenesis. *Circ Res*. 2007;100:70–78. doi: [10.1161/01.RES.0000254788.47304.6e](https://doi.org/10.1161/01.RES.0000254788.47304.6e)
67. Lahmann I, Bröhl D, Zyrianova T, Isomura A, Czajkowski MT, Kapoor V, Griger J, Ruffault PL, Mademtzoglou D, Zammit PS, et al. Oscillations of MyoD and Hes1 proteins regulate the maintenance of activated muscle stem cells. *Genes Dev*. 2019;33:524–535. doi: [10.1101/gad.322818.118](https://doi.org/10.1101/gad.322818.118)
68. Munk R, Martindale JL, Yang X, Yang JH, Grammatikakis I, Di Germanio C, Mitchell SJ, de Cabo R, Lehmann E, Zhang Y, et al. Loss of miR-451a enhances SPARC production during myogenesis. *PLoS One*. 2019;14:e0214301. doi: [10.1371/journal.pone.0214301](https://doi.org/10.1371/journal.pone.0214301)
69. Granata C, Oliveira RS, Little JP, Renner K, Bishop DJ. Mitochondrial adaptations to high-volume exercise training are rapidly reversed after a reduction in training volume in human skeletal muscle. *FASEB J*. 2016;30:3413–3423. doi: [10.1096/fj.201500100R](https://doi.org/10.1096/fj.201500100R)
70. Nieminen T, Toivanen PI, Laakkonen JP, Heikura T, Kaikkonen MU, Airene KJ, Yla-Herttuala S. Slit2 modifies VEGF-induced angiogenic responses in rabbit skeletal muscle via reduced eNOS activity. *Cardiovasc Res*. 2015;107:267–276. doi: [10.1093/cvr/cvv161](https://doi.org/10.1093/cvr/cvv161)
71. Perez-Cremades D, Cheng HS, Feinberg MW. Noncoding RNAs in critical limb ischemia. *Arterioscler Thromb Vasc Biol*. 2020;40:523–533. doi: [10.1161/ATVBAHA.119.312860](https://doi.org/10.1161/ATVBAHA.119.312860)
72. Caporali A, Meloni M, Vollenkle C, Bonci D, Sala-Newby GB, Addis R, Spinetti G, Losa S, Masson R, Baker AH, et al. Deregulation of microRNA-503 contributes to diabetes mellitus-induced impairment of endothelial function and reparative angiogenesis after limb ischemia. *Circulation*. 2011;123:282–291. doi: [10.1161/CIRCULATIONAHA.110.952325](https://doi.org/10.1161/CIRCULATIONAHA.110.952325)
73. Shi L, Fisslthaler B, Zippel N, Fromel T, Hu J, Elgheznawy A, Heide H, Popp R, Fleming I. MicroRNA-223 antagonizes angiogenesis by targeting beta1 integrin and preventing growth factor signaling in endothelial cells. *Circ Res*. 2013;113:1320–1330. doi: [10.1161/CIRCRESAHA.113.301824](https://doi.org/10.1161/CIRCRESAHA.113.301824)
74. Ghosh G, Subramanian IV, Adhikari N, Zhang X, Joshi HP, Basi D, Chandrashekar YS, Hall JL, Roy S, Zeng Y, Ramakrishnan S. Hypoxia-induced microRNA-424 expression in human endothelial cells regulates HIF-alpha isoforms and promotes angiogenesis. *J Clin Invest*. 2010;120:4141–4154. doi: [10.1172/JCI42980](https://doi.org/10.1172/JCI42980)
75. Zaccagnini G, Maimone B, Di Stefano V, Fasanaro P, Greco S, Perfetti A, Capogrossi MC, Gaetano C, Martelli F. Hypoxia-induced miR-210 modulates tissue response to acute peripheral ischemia. *Antioxid Redox Signal*. 2014;21:1177–1188. doi: [10.1089/ars.2013.5206](https://doi.org/10.1089/ars.2013.5206)
76. Ismael A, Fletcher E, Miserlis D, Wechsler M, Papoutsis E, Haynatzki G, Smith RS, Bohannon WT, Koutakis P. Skeletal muscle MiR-210 expression is associated with mitochondrial function in peripheral artery disease patients. *Transl Res*. 2022;246:66–77. doi: [10.1016/j.trsl.2022.03.003](https://doi.org/10.1016/j.trsl.2022.03.003)
77. Mohler ER III, Hiatt WR, Creager MA. Cholesterol reduction with atorvastatin improves walking distance in patients with peripheral arterial disease. *Circulation*. 2003;108:1481–1486. doi: [10.1161/01.CIR.0000090686.57897.F5](https://doi.org/10.1161/01.CIR.0000090686.57897.F5)
78. Henderson RM, Lovato L, Miller ME, Fielding RA, Church TS, Newman AB, Buford TW, Pahor M, McDermott MM, Stafford RS, et al. Effect of statin use on mobility disability and its prevention in at-risk older adults: the LIFE study. *J Gerontol A Biol Sci Med Sci*. 2016;71:1519–1524.

Supplemental Material

Table S1: mRNA primer sets

primer	sequence
MYBPH	F: 5'-AGTATCAGAGTCCACCAGAGAAG -3' R: 5'-TGCAGGCTTAGTGGCTGTG -3'
ACTC1	F: 5'-TCCCATCGAGCATGGTATCAT -3' R: 5'-GGTACGGCCAGAAGCATACA -3'
CDKN1A	F: 5'-TGTCCGTCAGAACCCATGC -3' R: 5'-AAAGTCGAAGTTCATCGCTC -3'
PLA2G2A	F: 5'-ATGAAGACCCTCCTACTGTTGG -3' R: 5'-GCTTCCTTTCCTGTCGTCAACT -3'
MYOG	F: 5'-GGGGAAAACCTACCTGCCTGTC -3' R: 5'-AGGCGCTCGATGTACTGGAT -3'
NNMT	F: 5'-ATATTCTGCCTAGACGGTGTGA -3' R: 5'-TCAGTGACGACGATCTCCTTAAA -3'
HES1	F: 5'-TCAACACGACACCGGATAAC -3' R: 5'-GCCGCGAGCTATCTTTCTTCA -3'
HAS2	F: 5'-CTCTTTTGGACTGTATGGTGCC -3' R: 5'-AGGGTAGGTTAGCCTTTTCACA -3'
XAF1	F: 5'-GCTCCACGAGTCCTACTGTG -3' R: 5'-GTTCACTGCGACAGACATCTC -3'
ITGA8	F: 5'-TCAGGCGTTCAACCTGGAC -3' R: 5'-GCGTCGGGTATGTGGAAGTC -3'
IHNBA	F: 5'-CCTCCCAAAGGATGTACCCAA -3' R: 5'-CTCTATCTCCACATACCCGTTCT -3'
L32	F: 5'-GTC AAG GAG CTG GAA GTG CT -3' R: 5'-CTC TTT CCA CGA TGG CTT TG -3'

Table S2: miRNA primer sets

primer	Cat. No.
hsa-miR-503-5p	YP00204334
hsa-miR-223-3p	YP00205986
hsa-miR-542-3p	YP00205444
hsa-miR-450b-5p	YP00205607
hsa-miR-135a-5p	YP00204762
hsa-miR-130b-3p	YP00204317
U6 SN RNA (v2)	YP02119464

Table S3. Differential expression genes (adj pvalue < 0.05).**PAD progression vs Non-PAD.**

gene_name	log2foldchange	pvalue	padjust
MYBPH	3.56323314	3.14E-13	5.09E-09
ACTC1	3.40807923	1.19E-08	4.83E-05
CDKN1A	2.32896987	6.02E-09	4.83E-05
RRAD	2.04899041	1.02E-08	4.83E-05
PLA2G2A	3.15141829	1.91E-08	6.20E-05
MYOG	1.24519907	2.86E-08	7.72E-05
NNMT	2.10839298	3.86E-08	8.93E-05
HES1	1.61129228	8.52E-08	0.00017251
CYR61	1.34985799	1.02E-07	0.00017268
RET	-1.3892857	1.07E-07	0.00017268
IGSF22	2.56349568	2.05E-07	0.00030256
IFITM10	2.88001595	4.79E-07	0.00059659
ANKRD1	2.26152774	4.56E-07	0.00059659
TNFRSF12A	1.89446708	5.49E-07	0.00063592
TCIM	-1.5059867	8.31E-07	0.00089803
HSPB1	2.03845933	1.56E-06	0.00157966
METTL7B	2.24417455	1.82E-06	0.00172525
MAGIX	1.38054113	1.92E-06	0.00172525
OAS3	-1.6941688	2.82E-06	0.00240808
JPT1	1.15235076	3.73E-06	0.00302142
PFKP	1.36896151	4.73E-06	0.00364836
RELB	1.55371129	5.53E-06	0.00407271
SORT1	0.81118309	7.71E-06	0.00543131
AL022323.1	1.63729604	8.35E-06	0.00563553
MIR503HG	2.75901297	1.11E-05	0.00612503
PIM1	1.57898965	9.72E-06	0.00612503
XIRP1	1.54964787	1.13E-05	0.00612503
AVPI1	1.32281973	1.12E-05	0.00612503

AC104083.1	-1.305126	1.06E-05	0.00612503
GUCA1B	-1.3155593	1.12E-05	0.00612503
JMJD4	1.43224826	1.40E-05	0.00675319
ADPRHL1	0.93038793	1.30E-05	0.00675319
RHOJ	-0.8104624	1.41E-05	0.00675319
ESR1	-1.0324932	1.42E-05	0.00675319
BTN3A1	-1.0795872	1.50E-05	0.00695246
VSIG10	-0.6811316	1.58E-05	0.00712614
SMCO4	1.44956928	1.63E-05	0.00713235
UBTD1	1.04546024	1.74E-05	0.00743972
ATP6V1FNB	1.80951518	1.91E-05	0.00794638
TDRD6	-1.277205	2.41E-05	0.00978203
TM4SF19	2.43781389	2.49E-05	0.00984367
AC004556.1	6.98977934	2.92E-05	0.01013591
FGFBP2	2.64701876	2.86E-05	0.01013591
MYL5	1.3865659	2.85E-05	0.01013591
SEC61A1	0.69463258	2.94E-05	0.01013591
PDP1	-1.0985077	2.81E-05	0.01013591
MUC3A	-1.2595795	2.83E-05	0.01013591
MAP3K20-AS1	1.54928274	3.32E-05	0.01114107
CSPG4	1.29850663	3.37E-05	0.01114107
GREB1	-1.2528006	3.48E-05	0.01126451
ITGA8	-1.534041	3.84E-05	0.01221387
ATOH8	1.46583419	4.23E-05	0.01245321
PLEKHO1	1.04338921	4.13E-05	0.01245321
HELZ2	-1.0813292	4.19E-05	0.01245321
IFI44L	-1.5323067	4.15E-05	0.01245321
DUSP8	0.94376848	4.35E-05	0.01258163
OTOF	1.88696999	4.50E-05	0.01264045
SLFN11	-0.8582215	4.52E-05	0.01264045
FXYD6	-1.1906106	4.63E-05	0.01272032
PLA1A	1.60398636	4.91E-05	0.01313699

PQLC2	1.06447528	4.95E-05	0.01313699
FAM174B	0.86794247	5.60E-05	0.01462986
RUNX1	1.53486698	5.83E-05	0.01500248
CRYAB	1.30806002	6.08E-05	0.01538977
RAPGEF5	-1.3429871	6.23E-05	0.01553934
KLHL30-AS1	0.96907809	6.40E-05	0.01570733
DOK7	1.11251979	7.18E-05	0.01736008
CHAC1	2.19371095	7.53E-05	0.01792329
GADD45A	1.27057021	7.63E-05	0.01792329
HIST1H1C	1.1268417	7.94E-05	0.01812396
KCND3	-1.0374544	7.88E-05	0.01812396
XAF1	-1.724895	8.32E-05	0.01871476
AC104574.2	4.22655749	8.56E-05	0.0190091
S100A8	2.70374173	8.79E-05	0.01925395
FGF6	1.47971285	9.96E-05	0.02123706
AVPR1A	-1.4726392	9.95E-05	0.02123706
AC108673.3	1.53359871	0.0001012	0.02129787
SLC6A1	-1.4547806	0.00010866	0.02257511
AKR1B10	1.33724834	0.00011259	0.02309606
ASCL5	2.09756597	0.00011669	0.02331013
PNMA8A	1.21600828	0.00011795	0.02331013
LIN52	-0.8097177	0.00011635	0.02331013
ITGA7	0.57650191	0.00012431	0.02426934
GDNF	1.52439717	0.00013102	0.02527653
RASD1	1.18146385	0.00013738	0.02529847
AK1	0.89731648	0.00013655	0.02529847
BIN1	0.81695817	0.00013697	0.02529847
RSAD2	-1.0615315	0.00013506	0.02529847
CAPN5	-0.9496133	0.0001401	0.02551004
PPP1R27	1.24565715	0.00014663	0.02640165
ST20-AS1	1.27673466	0.00015563	0.02741441
ZNF519	-1.2728385	0.00015564	0.02741441

KITLG	-1.2637183	0.00015998	0.02787557
NELFE	0.96745681	0.00016197	0.02792219
NIPSNAP1	-1.0427409	0.00016756	0.02858186
VGLL2	1.22365047	0.00018603	0.0314028
LTK	2.3759892	0.00022432	0.03228448
CGREF1	1.90673506	0.0002311	0.03228448
CTXND1	1.79309666	0.00021325	0.03228448
LIMK1	1.64817444	0.00021004	0.03228448
NQO1	1.57100638	0.0002266	0.03228448
ZNHIT2	1.56246542	0.00022466	0.03228448
EXOSC4	1.54086	0.00020582	0.03228448
AKR1C1	1.46492517	0.0002039	0.03228448
JAK3	1.32982365	0.00022896	0.03228448
DMPK	1.18119592	0.00021725	0.03228448
ADORA1	1.16128759	0.00021209	0.03228448
JUND	0.90101605	0.00023013	0.03228448
SERTAD3	0.89669267	0.00019653	0.03228448
RUNX1T1	-0.8791635	0.00022873	0.03228448
ITGA6	-0.9189098	0.00022574	0.03228448
PPM1K	-1.0588769	0.00022819	0.03228448
RGS5	-1.0753099	0.00021651	0.03228448
HERC6	-1.1229155	0.00020587	0.03228448
DACH1	-1.1816344	0.00019473	0.03228448
LINC01197	-1.83923	0.00021865	0.03228448
MYL6	0.99589594	0.00023385	0.03238854
HSPB7	0.77145534	0.00023989	0.03294468
HIST1H3E	-1.4751834	0.00024195	0.03294764
CDC42EP3	0.83665346	0.0002483	0.03325433
PLAGL1	-0.9611732	0.00024644	0.03325433
MT2A	1.71767414	0.00025245	0.03353169
TMEM189	0.82758329	0.00025957	0.03419735
ENTPD3	-1.6746954	0.0002661	0.03477556

ACTR1A	0.71432775	0.00027081	0.03510814
CEBPA	1.68744747	0.00027317	0.03513264
AKR1C2	1.72782718	0.00028136	0.03590166
PRRT3-AS1	1.3495623	0.00028856	0.03653245
AFAP1L2	-0.9394341	0.00029176	0.03665042
AL031590.1	2.41542393	0.00030234	0.03768823
FAM171B	-1.3991353	0.00030471	0.0376928
FNDC4	2.10464411	0.00030978	0.03774429
OXCT1	-1.1244141	0.00030791	0.03774429
HAS2	-2.0328986	0.0003139	0.03796113
MYOD1	0.97699194	0.00031844	0.03822412
SQOR	1.02908185	0.00032425	0.03863562
RNF150	-0.9019409	0.00033122	0.03917864
MMP24OS	1.03711363	0.00033758	0.03935364
LXN	-1.0263093	0.00033643	0.03935364
SLIT2	-1.1215136	0.00033999	0.03935364
SCAND1	1.4845905	0.00034348	0.03947522
S100A2	2.16763653	0.00036213	0.04028514
CHEK2	1.93646788	0.00036486	0.04028514
CTSD	1.68992494	0.00038316	0.04028514
ATF3	1.49667253	0.00038781	0.04028514
RIN1	1.35313423	0.00037012	0.04028514
AMPD3	1.1056534	0.00038659	0.04028514
MAP3K14	1.05343221	0.00035407	0.04028514
RUVBL2	1.02908536	0.00037278	0.04028514
AC020916.1	0.9775253	0.00037687	0.04028514
RARA	0.91928431	0.00038534	0.04028514
ZBTB40	-0.6020496	0.00037425	0.04028514
ZNF251	-0.6115635	0.00038178	0.04028514
SLC16A7	-1.3421763	0.00038229	0.04028514
AC074141.1	-1.521821	0.00038691	0.04028514
APCDD1L	-1.6181629	0.00037366	0.04028514

CREB5	1.05777116	0.0003918	0.04044066
HSPB1P1	2.04703536	0.00040062	0.04108912
STK40	0.72815013	0.00040408	0.04118268
EEF2KMT	0.96913137	0.00041231	0.04175919
MFGE8	0.80203379	0.00041634	0.04190587
FTLP15	2.79232317	0.00041931	0.04194433
CHST3	0.84167537	0.00043602	0.04294247
APO02761.4	0.67728807	0.00043235	0.04294247
BCKDHB	-0.8068094	0.00043814	0.04294247
SLC2A12	-1.0674921	0.00043989	0.04294247
CYP4F35P	-1.4709138	0.00044356	0.04304166
PPME1	0.62887708	0.00046252	0.04435022
PROS1	-0.6779803	0.00046239	0.04435022
IL17RD	-1.1524155	0.00046541	0.04436438
AC017104.4	-1.285144	0.0004691	0.04445506
ARPC4	1.24515402	0.00048148	0.04536259
ZNF358	1.35180768	0.00049266	0.04614743
CLCF1	1.79021808	0.00051073	0.04664969
H1FX	1.47150399	0.00051241	0.04664969
CHRNA1	1.32812283	0.00050435	0.04664969
ITGAL	1.11975858	0.00050739	0.04664969
1-sep	1.08057795	0.00050293	0.04664969
SDHAF2	1.14039711	0.00053218	0.04817849
TMEM238	1.85080902	0.00054252	0.04884206
PQLC1	1.0084411	0.00054847	0.04910458
SERGEF	1.05065286	0.00055202	0.04915078
HSPB8	0.77401974	0.00056358	0.04963493
NPHP1	-0.8547318	0.00056258	0.04963493
COL15A1	-0.9214258	0.00056799	0.04975298

PAD no progression vs Non PAD.

gene_name	log2foldchange	pvalue	padjust
ACOT11	-1.1821704	2.80E-07	0.00305
DKK2	-1.7881628	2.09E-07	0.00305
MTND1P23	-6.9448243	1.04E-06	0.00752707

PAD progression vs PAD no progression.

gene_name	log2foldchange	pvalue	padjust
MTND1P23	7.33737384	4.82E-09	7.70E-05
OAS3	-1.4840759	3.50E-08	0.00027937
HIST1H3E	-2.5956997	1.86E-07	0.00099339
AKR1B10	1.857671	1.26E-06	0.0050386
HSPB1P1	2.25922051	6.95E-06	0.02220754
IFI44L	-1.5000827	1.14E-05	0.02607493
RRP12	1.30740578	1.10E-05	0.02607493
AC020637.1	2.98201455	1.49E-05	0.02969972

Table S4.**Significant biological pathways associated with differentially expressed genes (adj p < 0.05) between PAD progression and non-PAD group.**

#	Networks	p-value	FDR	Hits	Network Objects from Active Data
1	Muscle contraction	1.5835E-08	2.0586E-06	14	MRLC, MYBPH, Alpha crystallin B, ACTC, GCAP2, Smooth muscle myosin, Actin muscle, nAChR alpha, MELC, nAChR alpha-1, Galpha(q)-specific peptide GPCRs, DMPK, GCAP, Actin
2	Development_Skeletal muscle development	9.8771E-07	6.4201E-05	11	MRLC, VGL-3, MYBPH, Alpha crystallin B, Smooth muscle myosin, Actin muscle, MELC, MYOG, Actin, MYOD, ITGA7
3	Cytoskeleton_Actin filaments	0.00025227	0.01093175	9	MRLC, RhoJ, ACTC, ARPC4, Actin muscle, MELC, LIMK1, Nephrocystin, Actin
4	Reproduction_Feeding and Neurohormone signaling	0.00091653	0.02724331	9	HSP27, AKR1C1, Pim-1, Integrin, ITGAL, MGF, Histone H3, Galpha(q)-specific peptide GPCRs, Cathepsin D
5	Cell adhesion_Integrin-mediated cell-matrix adhesion	0.00104782	0.02724331	9	MRLC, ITGA8, ITGA6, Integrin, Cyr61, MELC, LIMK1, Actin, ITGA7
6	Cytoskeleton_Regulation of cytoskeleton rearrangement	0.00157137	0.03404626	8	MRLC, RhoJ, ACTC, ARPC4, Actin muscle, MELC, LIMK1, Actin
7	Signal Transduction_TGF-beta, GDF and Activin signaling	0.00249186	0.04627739	7	p21, AP-1, Integrin, C/EBPalpha, MYOG, MYOD, JunD
8	Inflammation_Amphoterin signaling	0.00292311	0.04750052	6	MRLC, AP-1, Calgranulin A, MELC, LIMK1, Actin
9	Signal Transduction_BMP and GDF signaling	0.00450504	0.06507287	5	p21, C/EBPalpha, MYOG, MYOD, JunD
10	Apoptosis_Apoptotic nucleus	0.01295634	0.1544716	6	p21, Histone H3, Histone H1, Zac1, GADD45 alpha, Chk2
11	Inflammation_IL-6 signaling	0.0142721	0.1544716	5	p21, AP-1, JAK3, C/EBP, C/EBPalpha
12	Signal transduction_ESR1-nuclear pathway	0.01522298	0.1544716	7	p21, HSP27, ESR1 (nuclear), RARalpha, Zac1, SDP1, Cathepsin D
13	DNA damage_Checkpoint	0.01679321	0.1544716	5	p21, ATF-3, RUVBL2, GADD45 alpha, Chk2
14	Immune response_Phagocytosis	0.0178473	0.1544716	7	MRLC, Adenosine A1 receptor, MFGE8, C/EBP, MELC, LIMK1, Actin
15	Cell adhesion_Attractive and repulsive receptors	0.0183777	0.1544716	6	SLIT2, ITGA6, Integrin, ITGAL, LIMK1, Actin
16	Cell cycle_G1-S Interleukin regulation	0.01901189	0.1544716	5	p21, AP-1, JAK3, RelB (NF-kB subunit), NIK(MAP3K14)
17	Chemotaxis	0.0260862	0.1994827	5	SLIT2, Integrin, Cyr61, Galpha(q)-specific peptide GPCRs, AML1 (RUNX1)
18	Development_Keratinocyte differentiation	0.03264042	0.2257126	3	p21, C/EBPalpha, JunD
19	Cell cycle_S phase	0.03298876	0.2257126	5	p21, Histone H3, Histone H1, GADD45 alpha, Chk2
20	Inflammation_IL-2 signaling	0.03670573	0.234643	4	ESR1 (nuclear), AP-1, JAK3, ESR
21	Cell cycle_G2-M	0.03790387	0.234643	6	MRLC, p21, Histone H3, Histone H1, GADD45 alpha, Chk2
22	Inflammation_Protein C signaling	0.04127422	0.24389314	4	Protein S, NIK(MAP3K14), LIMK1, Actin
23	Reproduction_Progesterone signaling	0.04514801	0.24819103	6	ESR1 (nuclear), AP-1, PLA2, ESR1 (membrane), Galpha(q)-specific peptide GPCRs, Chk2
24	Cell adhesion_Glycoconjugates	0.04581988	0.24819103	5	HAS, Integrin, HAS2, LIMK1, Actin

Significant biological pathways associated with differentially expressed genes ($p < 0.05$) between PAD no progression and non-PAD group.

#	Networks	p-value	FDR	Hits	Network Objects from Active Data
1	Muscle contraction	2.0017E-07	2.6463E-05	20	K(+) channel, subfamily J, MELC, Myosin II, ACTC, Galpha(i)-specific peptide GPCRs, MyHC, CFTR, nAChR alpha-1, Actin, Alpha-actinin 2, MYL4, Alpha-actinin, G-protein alpha-i family, nAChR delta, Galpha(q)-specific peptide GPCRs, MRLC, MYBPH, Alpha-actinin 3, Actin muscle, nAChR
2	Cell adhesion_Integrin-mediated cell-matrix adhesion	3.4819E-07	2.6463E-05	22	Syndecan-4, ITGA2B, Galectin-1, MELC, ERM proteins, Integrin, MyHC, Tcf(Lef), TM4SF9, Cyclin D1, Actin, Alpha-actinin 2, PI3K cat class IA, Alpha-actinin, CDEP, VAV-1, MRLC, ITGA8, PI3K cat class IA (p110-delta), Alpha-actinin 3, Cyr61, VIL2 (ezrin)
3	Signal transduction_WNT signaling	5.0017E-06	0.00025342	18	ESR1 (nuclear), Cyclin D2, Cyclin A2, p63, HES1, Tcf(Lef), PP2A regulatory, EGF, Cyclin D1, FZD2, G-protein alpha-i family, FZD5, Lef-1, Adenylate cyclase, TCF7 (TCF1), Frizzled, G-protein alpha-o, WISP2
4	Cytoskeleton_Regulation of cytoskeleton rearrangement	8.0121E-06	0.00030446	18	CD43, MELC, Myosin II, ERM proteins, ACTC, MyHC, Actin, Alpha-actinin 2, Alpha-actinin, Galpha(i)-specific amine GPCRs, G-protein alpha-i family, VAV-1, MRLC, G-protein alpha-o, Alpha-actinin 3, Actin muscle, VIL2 (ezrin), 14-3-3
5	Cell adhesion_Platelet aggregation	1.8033E-05	0.00048917	16	PLA2, MELC, Myosin II, MyHC, PF4, Alpha-actinin 2, PI3K cat class IA, Alpha-actinin, G-protein alpha-i family, Adenylate cyclase, VAV-1, MRLC, PI3K cat class IA (p110-delta), Slp76, Alpha-actinin 3, Adenylate cyclase type VII
6	Cell cycle_G1-S Growth factor regulation	1.931E-05	0.00048917	18	p21, Cyclin D2, Cyclin A2, p16INK4, PPP2R2B, STAT5, Tcf(Lef), PP2A regulatory, Cyclin A, EGF, Cyclin D1, p14ARF, PI3K cat class IA, G-protein alpha-i family, FGF6, RelB (NF-kB subunit), PI3K cat class IA (p110-delta), Cyclin D
7	Development_Hemopoiesis, Erythropoietin pathway	5.0845E-05	0.00110406	14	Cyclin D2, Cyclin A2, STAT5A, STAT5, Cyclin A, HBB, Cyclin D1, PI3K cat class IA, Pim-1, CISH, TRPC2, VAV-1, PI3K cat class IA (p110-delta), Cyclin D
8	Reproduction_Feeding and Neurohormone signaling	0.00017123	0.00325345	17	Cyclin D2, Galpha(q)-specific Class A Orphan/other GPCRs, STAT5A, Galpha(i)-specific peptide GPCRs, STAT5, Integrin, ITGAL, PP2A regulatory, PI3K cat class IA, G-protein alpha-i family, Pim-1, Galpha(q)-specific peptide GPCRs, MSP receptor (RON), GLI-1, G-protein alpha-o, Histone H3, IBP3
9	Inflammation_IL-10 anti-inflammatory response	0.00024934	0.00380377	10	Cyclin D2, Cyclin A2, STAT5A, STAT5, PF4, Cyclin D1, PI3K cat class IA, Pim-1, PI3K cat class IA (p110-delta), Cyclin D
10	Chemotaxis	0.00025025	0.00380377	13	CD43, pp12/A4, CCR3, Galpha(i)-specific peptide GPCRs, Integrin, PF4, PI3K cat class IA, CCR1, G-protein alpha-i family, Galpha(q)-specific peptide GPCRs, CCR7, Cyr61, AML1 (RUNX1)
11	Proliferation_Positive regulation cell proliferation	0.00031522	0.00435578	17	p21, CCR3, IL-31RA, Bcl-6, Dexras1, Galpha(i)-specific peptide GPCRs, EGF, Cyclin D1, PI3K cat class IA, Galpha(i)-specific amine GPCRs, CCR1, G-protein alpha-i family, Rap1GAP1, MSP receptor (RON), MRLC, PI3K cat class IA (p110-delta), VEGF-C
12	Cell cycle_G1-S Interleukin regulation	0.00042313	0.00535961	12	p21, Cyclin D2, Cyclin A2, p16INK4, STAT5, Cyclin A, Cyclin D1, p14ARF, PI3K cat class IA, RelB (NF-kB subunit), PI3K cat class IA (p110-delta), Cyclin D
13	Cytoskeleton_Actin filaments	0.00076805	0.00898026	14	MELC, Myosin II, ERM proteins, ACTC, MyHC, MYH10, Actin, Alpha-actinin 2, Alpha-actinin, MRLC, Alpha-actinin 3, Actin muscle, Nephrocystin, VIL2 (ezrin)
14	Cell adhesion_Cadherins	0.00112577	0.01222263	14	Cadherin 8, RET, PTPRF (LAR), DKK2, Tcf(Lef), MAST205, Actin, Alpha-actinin 2, PI3K cat class IA, Alpha-actinin, Reelin, Frizzled, WISP2, Alpha-actinin 3

15	Development_Blood vessel morphogenesis	0.00122013	0.01236402	16	ANGPTL4, Galpha(i)-specific peptide GPCRs, STAT5, KLF5, PF4, EGF, PI3K cat class IA, Galpha(i)-specific amine GPCRs, CCR1, G-protein alpha-i family, Galpha(q)-specific peptide GPCRs, RelB (NF-kB subunit), VEGF-C, F263, Cyr61, Transferrin
16	Signal transduction_ESR1-membrane pathway	0.00151883	0.01433405	9	ESR1 (nuclear), Cyclin D2, ESR1 (membrane), EGF, Cyclin D1, PI3K cat class IA, G-protein alpha-i family, Adenylate cyclase, Adenylate cyclase type VII
17	Apoptosis_Anti-Apoptosis mediated by external signals via PI3K/AKT	0.00160315	0.01433405	16	Bcl-6, GDNF, RAET1E, c-IAP2, PP2A regulatory, EGF, PI3K cat class IA, BDNF, Caspase-7, G-protein alpha-i family, Adenylate cyclase, Beta-2 adrenergic receptor, FGF6, G-protein alpha-o, VEGF-C, Adenylate cyclase type VII
18	Reproduction_Progesterone signaling	0.0019118	0.01614409	15	ESR1 (nuclear), PLA2, ESR1 (membrane), Cyclin A2, Chk2, Tcf(Lef), Cyclin A, EGF, PI3K cat class IA, G-protein alpha-i family, AKAP3, Lef-1, Adenylate cyclase, Galpha(q)-specific peptide GPCRs, Frizzled
19	Cell adhesion_Leucocyte chemotaxis	0.00280773	0.02246182	13	CCR3, Galpha(i)-specific peptide GPCRs, PI3K cat class IA, Alpha-actinin, ITK, CCR1, G-protein alpha-i family, Rap1GAP1, Galpha(q)-specific peptide GPCRs, VAV-1, PI3K cat class IA (p110-delta), Slp76, CCR7
20	Inflammation_IL-2 signaling	0.00381207	0.02897175	9	ESR1 (nuclear), Cyclin D2, STAT5A, STAT5, PI3K cat class IA, CCR1, CISH, ESR, PI3K cat class IA (p110-delta)
21	Immune response_Phagocytosis	0.00687431	0.04975689	14	MELC, Myosin II, ERM proteins, MyHC, Actin, Alpha-actinin 2, PI3K cat class IA, Alpha-actinin, VAV-1, MRLC, PI3K cat class IA (p110-delta), Slp76, Alpha-actinin 3, VIL2 (ezrin)
22	Development_Neurogenesis_Axonal guidance	0.0086134	0.05760145	14	SLIT3, MELC, ERM proteins, Integrin, Semaphorin 5A, MyHC, MYH10, Actin, PI3K cat class IA, Reelin, BDNF, NRCAM, DCAMKL1, Plexin A4
23	Development_Hedgehog signaling	0.00871601	0.05760145	15	p21, p63, HOXA13, HES1, Cyclin D1, HIP, FZD2, G-protein alpha-i family, FZD5, Lef-1, Adenylate cyclase, GLI-1, Frizzled, G-protein alpha-o, Adenylate cyclase type VII
24	Cell cycle_G1-S	0.00914202	0.05789946	11	p21, Cyclin D2, Cyclin A2, p16INK4, Chk2, Cyclin A, 14-3-3 sigma, Cyclin D1, p14ARF, Cyclin D, 14-3-3
25	Development_Skeletal muscle development	0.01044774	0.06352226	10	Myostatin, Collagen V, MELC, Myosin II, MyHC, Actin, MYL4, MRLC, MYBPH, Actin muscle
26	DNA damage_Checkpoint	0.01180511	0.06901451	9	p21, Cyclin D2, Cyclin A2, Chk2, Cyclin A, 14-3-3 sigma, Cyclin D1, Cyclin D, 14-3-3
27	Signal Transduction_Cholecystokinin signaling	0.01383324	0.07787603	8	ESR1 (nuclear), CCR3, Galpha(i)-specific peptide GPCRs, M-Ras, G-protein alpha-i family, Adenylate cyclase, Galpha(q)-specific peptide GPCRs, Adenylate cyclase type VII
28	Development_Regulation of angiogenesis	0.01506344	0.08177297	13	p21, ANGPTL4, ACTC, Galpha(i)-specific peptide GPCRs, STAT5, Semaphorin 5A, PF4, PI3K cat class IA, CCR1, G-protein alpha-i family, Galpha(q)-specific peptide GPCRs, GLI-1, RelB (NF-kB subunit)
29	Apoptosis_Anti-apoptosis mediated by external signals via NF-kB	0.01785575	0.09358878	8	Bcl-6, c-IAP2, PP2A regulatory, PI3K cat class IA, Caspase-7, G-protein alpha-i family, Adenylate cyclase, FN14(TNFRSF12A)
30	Proliferation_Lymphocyte proliferation	0.02268365	0.11389787	12	p21, IL-2R gamma chain, Cyclin D2, CD43, STAT5A, STAT5, TEC, ICOS-L, PI3K cat class IA, VAV-1, PI3K cat class IA (p110-delta), Slp76
31	Cell adhesion_Glycoconjugates	0.02322917	0.11389787	10	CD43, Galectin-1, Galectin-4, Integrin, PF4, TEC, L-selectin, Actin, BDNF, NRCAM
32	Signal transduction_CREM pathway	0.02711866	0.12881361	7	Cyclin D2, Cyclin A2, EGF, AKAP3, Adenylate cyclase, Beta-2 adrenergic receptor, SYTL4
33	Transport_Calcium transport	0.02889141	0.13307559	11	Calgranulin A, NCKX3, CACNB2, PDP1, P2X3, nAChR alpha-1, nAChR delta, TRPC2, Otoferlin, Calsyntenin-1, Ca-ATPase2
34	Apoptosis_Apoptotic mitochondria	0.03045063	0.13613223	6	GDNF, CFTR, PI3K cat class IA, Glutaredoxin, 14-3-3, Glutaredoxin 1
35	Cell adhesion_Attractive and repulsive receptors	0.03565215	0.15483218	10	SLIT3, Galectin-1, Integrin, Semaphorin 5A, ITGAL, Actin, PI3K cat class IA, NRCAM, PI3K cat class IA (p110-delta), Plexin A4

36	Cell adhesion_Synaptic contact	0.03936865	0.1662232	10	K(+) channel, subfamily J, Alpha-actinin 2, Alpha-actinin, SHANK, SHANK2, Calsyntenin-1, Alpha-actinin 3, GluR1, SHANK1, DLGAP3 (SAPAP3)
37	Signal Transduction_TGF-beta, GDF and Activin signaling	0.04114131	0.16901295	9	p21, Cyclin D2, Myostatin, Integrin, PP2A regulatory, Cyclin D1, PI3K cat class IA, Lef-1, VAV-1
38	Cell cycle_Meiosis	0.04270597	0.17082388	7	Myelin basic protein, PP2A regulatory, Cyclin A, EGF, 14-3-3 sigma, PI3K cat class IA, 14-3-3
39	Cell cycle_G2-M	0.04466214	0.17406784	11	p21, Cyclin A2, Myosin II, Chk2, Cyclin A, EGF, 14-3-3 sigma, MRLC, TXNL4B, Histone H3, 14-3-3
40	Cardiac development_Role of NADPH oxidase and ROS	0.04737943	0.17641895	8	NOX4, ESR1 (nuclear), Bcl-6, HEXIM1, MyHC, MYH10, Caspase-7, DHA2
41	Proliferation_Negative regulation of cell proliferation	0.04758669	0.17641895	10	p21, Galpha(i)-specific peptide GPCRs, Cyclin D1, PI3K cat class IA, CCR1, G-protein alpha-i family, IBP, IL6RA, IBP3, CGR11

Significant biological pathways associated with differentially expressed genes (p < 0.05) between PAD progression and PAD no progression group.

#	Networks	p-value	FDR	Hits	Network Objects from Active Data
1	Development_Skeletal muscle development	8.9827E-08	1.4193E-05	24	Alpha crystallin B, HB-EGF, Myosin II, FHL3, MYL4, Syntrophin A, ANKRD2, Collagen IV, p38gamma (MAPK12), MELC, CRP3 (MLP), MyHC, Actin, VGL-3, p38 MAPK, MRLC, MURF2, Filamin C, Actin muscle, Lamin A/C, MYOG, alpha-MHC, MYOD, ITGA7
2	Cytoskeleton_Regulation of cytoskeleton rearrangement	7.8403E-07	6.1938E-05	26	Plectin 1, Profilin I, Tubulin gamma, Dematin, Myosin II, ARPC1A, ACTC, ROCK, Band 4.1-like protein 2, PARD3, Profilin, CAS-L, RhoJ, MELC, LIMK1, Tubulin gamma 1, ARPC1, MyHC, Actin, ECT2, Zyxin, MRLC, ROCK1, ARPC4, Filamin C, Actin muscle
3	Cytoskeleton_Actin filaments	4.4086E-06	0.00023219	24	Plectin 1, Profilin I, Dematin, Myosin II, ARPC1A, ACTC, ROCK, Band 4.1-like protein 2, Profilin, CAS-L, RhoJ, MELC, LIMK1, DAAM1, CapG, ARPC1, MyHC, Actin, Zyxin, MRLC, ROCK1, ARPC4, Filamin C, Actin muscle
4	Muscle contraction	3.7102E-05	0.00146551	22	Alpha crystallin B, Myosin II, ACTC, HRC, ROCK, DMPK, MYL4, Syntrophin A, Galpha(q)-specific peptide GPCRs, MYBPC3, ANKRD2, G-protein alpha-q/11, Syntaxin 1A, MELC, GCAP, MyHC, Actin, MRLC, EDNRA, GCAP2, Actin muscle, alpha-MHC
5	Reproduction_Male sex differentiation	0.00031054	0.00981321	25	HB-EGF, HMGI/Y, Histone H2AX, STAT5A, STAT5, Par-4, G-protein alpha-q, Bax, p90RSK1, DEDD, G-protein alpha-q/11, p21, SHBG, HSP70, FASN, ATF-2, Tubulin gamma 1, Histone H2, Histone H2A, p38 MAPK, H-Ras, HSPA1A, RARalpha, Histone H1, Lamin A/C
6	Reproduction_Feeding and Neurohormone signaling	0.00058544	0.01375537	22	4E-BP1, STAT5A, AKR1C1, STAT5, G-protein alpha-q, Bax, MSP, Galpha(q)-specific peptide GPCRs, Histone H3, G-protein alpha-q/11, Endothelin-1, DCOR, MGF, HSP70, c-Kit, Antileukoproteinase 1, PP2A structural, HSP27, Pim-1, H-Ras, Cathepsin D, PREB
7	Protein folding_Response to unfolded proteins	0.00060941	0.01375537	11	UIP5, VCP, Kinesin light chain, HSP70, HSPB7, OSP94, HSP27, DNAJB2, HSPA1A, AMFR, HSPA1B
8	Signal transduction_WNT signaling	0.0010227	0.02019842	19	HB-EGF, Casein kinase II, beta chain (Phosvitin), G-protein alpha-q, WNT5A, G-protein alpha-q/11, CUX1, p38gamma (MAPK12), Fra-1, FRAT1, DAAM1, HES1, PP2A structural, WNT, p38 MAPK, NF-AT2(NFATC1), NF-AT, Frizzled, WNT6, MYOD
9	Inflammation_Amphoterin signaling	0.00180061	0.03161079	14	NFKBIB, I-kB, ROCK, p38gamma (MAPK12), MELC, LIMK1, MyHC, Actin, p38 MAPK, TLR4, H-Ras, NFKBIE, MRLC, ROCK1
10	Inflammation_IL-10 anti-inflammatory response	0.0033103	0.05230281	11	NFKBIB, Heme oxygenase 1, I-kB, STAT5A, STAT5, TIA-1, p38gamma (MAPK12), p38 MAPK, Pim-1, TLR4, NFKBIE
11	Cell adhesion_Integrin-mediated cell-matrix adhesion	0.00402702	0.05784262	20	CD151, Profilin I, ITGA1, ROCK, ITGA6, Profilin, Collagen IV, MELC, LIMK1, Myosin X, Osteonectin, MyHC, Actin, Zyxin, H-Ras, MRLC, ROCK1, Filamin C, RhoGDI alpha, ITGA7

12	Apoptosis_Apoptotic mitochondria	0.00496849	0.06080427	10	BAD, BOK, TIP30, Bax, PR65-alpha, NIP1, HSP70, BAG-3, ASK1 (MAP3K5), Cathepsin D
13	Apoptosis_Apoptotic nucleus	0.00539478	0.06080427	16	AHR, NRIF3, Ku70, Par-4, Bax, PREG3, GADD45 gamma, TIA-1, Histone H3, p21, NDPK A, MDA-5, Zac1, Histone H1, Lamin A/C, Proline oxidase 1
14	Inflammation_Inflammasome	0.00571918	0.06080427	13	CARD7, NFKBIB, I-kB, IL-18, p38gamma (MAPK12), MDA-5, TNF-R1, p38 MAPK, TLR4, NFKBIE, IL-33, CARD8, eIF2B4
15	Development_Regulation of angiogenesis	0.00577256	0.06080427	20	SPHK1, HB-EGF, I-kB, ACTC, STAT5, VEGFR-1, VEGFR-2, Galpha(q)-specific peptide GPCRs, RelB (NF-kB subunit), G-protein alpha-q/11, p21, IL-18, Endothelin-1, Osteonectin, RAI, H-Ras, Cathepsin B, EDNRA, PRK1, ITGA7
16	Inflammation_Protein C signaling	0.00638005	0.06300302	12	SPHK1, NFKBIB, I-kB, ROCK, NIK(MAP3K14), LIMK1, Protein S, Actin, Coagulation factor VIII, TLR4, NFKBIE, ROCK1
17	Development_Keratinocyte differentiation	0.00690604	0.06418554	8	GATA-3, G-protein alpha-q/11, p21, Fra-1, VDR, ASK1 (MAP3K5), H-Ras, C/EBPalpha
18	Cardiac development_FGF_ErbB signaling	0.00751585	0.0659725	13	HB-EGF, ECE2, MYBPC3, G-protein alpha-q/11, BARX2, Endothelin-1, MyHC, HAS2, ZFPM1 (FOG), H-Ras, EDNRA, RARalpha, alpha-MHC
19	Cardiac development_Wnt_beta-catenin, Notch, VEGF, IP3 and integrin signaling	0.015902	0.13223764	14	VEGFR-1, CMYA1, G-protein alpha-q, VEGFR-2, MYBPC3, G-protein alpha-q/11, CRP3 (MLP), HES1, MyHC, WNT, NF-AT2(NFATC1), GYS1, Frizzled, alpha-MHC
20	Inflammation_Histamine signaling	0.01815751	0.14187851	18	CCL5, NFKBIB, I-kB, ROCK, PTGIS, iPLA2, PA2G6, iNOS, G-protein alpha-q/11, IL-18, p38gamma (MAPK12), PLA2, LIMK1, Actin, p38 MAPK, NF-AT2(NFATC1), NFKBIE, ROCK1
21	Signal transduction_ESR1-nuclear pathway	0.01894852	0.14187851	18	NRIF3, BLOS1, STAT5A, VEGFR-2, CYP1B1, SDP1, p90RSK1, COMT, BARX2, p21, Zac1, HSD17B1, HSP27, MRF-1, H-Ras, p90Rsk, Cathepsin D, RARalpha
22	Apoptosis_Anti-apoptosis mediated by external signals via NF-kB	0.01975524	0.14187851	11	BAD, I-kB, OX40(TNFRSF4), VEGFR-2, NIK(MAP3K14), TNF-R1, PP2A structural, TLR4, H-Ras, p90Rsk, FN14(TNFRSF12A)
23	Cell adhesion_Platelet aggregation	0.02270566	0.15597798	14	GAB2, Myosin II, ROCK, ADAM-TS13, G-protein alpha-q, PTGIS, G-protein alpha-q/11, Collagen IV, PLA2, MELC, MyHC, Gab, MRLC, ROCK1
24	Immune response_Phagocytosis	0.02525484	0.16626104	18	Profilin I, MFGE8, NFKBIB, C/EBP, Myosin II, I-kB, ROCK, Profilin, p38gamma (MAPK12), MELC, LIMK1, MyHC, Actin, p38 MAPK, TLR4, NFKBIE, MRLC, ROCK1
25	DNA damage_DBS repair	0.02645812	0.16721534	11	Casein kinase II, beta chain (Phosvitin), Histone H2AX, Sirtuin, Ku70, RAD51L3, Histone H3, RUVBL2, PIR51, PP2A structural, Sirtuin7, NMP200
26	Inflammation_IL-2 signaling	0.03077133	0.18699498	10	BAD, NFKBIB, I-kB, STAT5A, STAT5, p38 MAPK, H-Ras, NF-AT2(NFATC1), NFKBIE, NF-AT
27	Reproduction_Spermatogenesis, motility and copulation	0.03555807	0.20808056	18	HB-EGF, MFGE8, HMGI/Y, Histone H2AX, STAT5A, STAT5, p90RSK1, SHBG, SPAG17, HSP70, ATF-2, HSP27, Histone H2, Histone H2A, H-Ras, HSPA1A, RARalpha, Histone H1
28	Signal Transduction_TGF-beta, GDF and Activin signaling	0.03870045	0.21195036	13	GATA-3, MECOM, p21, ATF-2, c-Kit, CtBP1, PP2A structural, p38 MAPK, H-Ras, C/EBPalpha, GDF9, MYOG, MYOD
29	DNA damage_Checkpoint	0.04038446	0.21195036	11	Heme oxygenase 1, Histone H2AX, I-kB, Ku70, GADD45 gamma, p21, p38gamma (MAPK12), RUVBL2, ATF-2, p38 MAPK, ANAPC7
30	Inflammation_IFN-gamma signaling	0.04063054	0.21195036	10	CCL5, NFKBIB, I-kB, iNOS, p21, IL-18, ATF-2, p38 MAPK, TLR4, NFKBIE
31	Inflammation_IgE signaling	0.0415852	0.21195036	12	GAB2, NFKBIB, I-kB, PTGIS, PLA2, ATF-2, p38 MAPK, H-Ras, NF-AT2(NFATC1), NFKBIE, CBR1, NF-AT
32	Proliferation_Positive regulation cell proliferation	0.043198	0.21329013	17	RhoG, GAB2, VEGFR-1, G-protein alpha-q, G-protein alpha-q/11, p21, Endothelin-1, Fra-1, MGF, ATF-2, c-Kit, H-Ras, ISG20, MRLC, Neuropilin-1, CSPG4 (NG2), EDNRA
33	Translation_Regulation of initiation	0.04672169	0.22369777	11	Casein kinase II, beta chain (Phosvitin), 4E-BP1, MNK2(GPRK7), G-protein alpha-q, G-protein alpha-q/11, p38gamma (MAPK12), HSP27, p38 MAPK, eIF3S9, H-Ras, eIF2B4

34	Apoptosis_Apoptosis stimulation by external signals	0.04977783	0.22862671	12	BAD, HB-EGF, Acid sphingomyelinase, I-kB, G-protein alpha-q, Bax, TNF-R1, FLASH, TrkC, ASK1 (MAP3K5), H-Ras, Cathepsin D
----	---	------------	------------	----	--

Table S5. Differential expression analysis**PAD progression vs Non PAD**

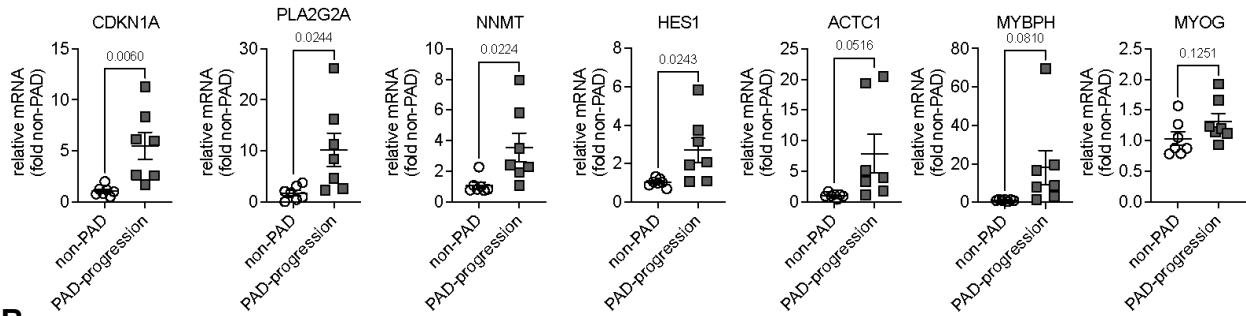
miRNAs	log2FC	PValue	FDR
hsa-miR-223-3p	1.41805585	3.26E-09	1.08E-06
hsa-miR-135a-5p	-2.1345353	2.68E-06	0.00044297
hsa-miR-503-5p	1.5216993	4.95E-06	0.00054494
hsa-miR-451a	1.0035613	1.67E-05	0.00138122
hsa-miR-142-5p	0.79598806	5.43E-05	0.00250688
hsa-miR-16-2-3p	0.8511787	3.99E-05	0.00250688
hsa-miR-450b-5p	1.20340263	5.38E-05	0.00250688
hsa-miR-542-3p	1.34129627	6.08E-05	0.00250688
hsa-miR-146a-5p	0.88474104	0.00010369	0.00342187
hsa-miR-424-5p	1.00660843	9.94E-05	0.00342187
hsa-miR-7-5p	0.67914456	0.0001639	0.00491693
hsa-miR-142-3p	0.74017088	0.00039054	0.00920552
hsa-miR-130b-3p	0.81332413	0.00038201	0.00920552
hsa-miR-942-5p	0.87370897	0.00035388	0.00920552
hsa-miR-141-3p	0.75041965	0.00054002	0.01113796
hsa-miR-542-5p	1.12163229	0.0005193	0.01113796
hsa-miR-25-3p	0.60617785	0.00070703	0.01372478
hsa-miR-15b-3p	0.69841591	0.00080068	0.01467908
hsa-miR-19b-3p	0.55332367	0.0009063	0.01574101
hsa-miR-452-5p	1.11680545	0.00137657	0.02271345
hsa-miR-21-3p	0.9485453	0.00173807	0.02731252
hsa-miR-93-5p	0.57612409	0.00280792	0.04211879
hsa-miR-185-5p	0.60779214	0.00298856	0.04287936
hsa-miR-629-5p	0.66591532	0.00319418	0.04391999
hsa-miR-19a-3p	0.53153065	0.00360498	0.04729794
hsa-miR-144-5p	0.645442	0.0037265	0.04729794

Table S6. miRNA-mRNA interaction analysis of PAD progression vs Non PAD groups. Differentially expressed (adjusted P<0.05) miRNAs and mRNAs were used to identify miRNA-mRNA pairings with opposite expression. miRNA target prediction databases and confidence filter are also shown.

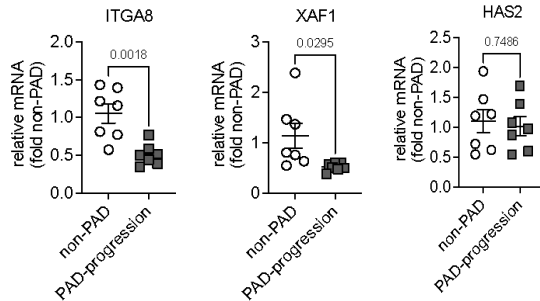
miRNA	log2FC	padj	Source	Confidence	mRNA	log2FC	padj
hsa-miR-503-5p	1.52	0.0005	TargetScan Human	Moderate (predicted)	RET	-1.39	0.0002
hsa-miR-424-5p	1.01	0.0034	TargetScan Human	Moderate (predicted)	RET	-1.39	0.0002
hsa-miR-7-5p	0.68	0.0049	TargetScan Human	Moderate (predicted)	OAS3	-1.69	0.0024
hsa-miR-21-3p	0.95	0.0273	TargetScan Human	Moderate (predicted)	GUCA1B	-1.32	0.0061
hsa-miR-503-5p	1.52	0.0005	TargetScan Human	Moderate (predicted)	RHOJ	-0.81	0.0068
hsa-miR-130b-3p	0.81	0.0092	TargetScan Human	High (predicted)	ESR1	-1.03	0.0068
hsa-miR-19b-3p	0.55	0.0157	TargetScan Human,miRecords	Experimentally Observed,High (predicted)	ESR1	-1.03	0.0068
hsa-miR-185-5p	0.61	0.0429	TargetScan Human	Moderate (predicted)	RHOJ	-0.81	0.0068
hsa-miR-142-3p	0.74	0.0092	TargetScan Human	Moderate (predicted)	ITGA8	-1.53	0.0122
hsa-miR-25-3p	0.61	0.0137	TargetScan Human	Moderate (predicted)	ITGA8	-1.53	0.0122
hsa-miR-25-3p	0.61	0.0137	TargetScan Human	Moderate (predicted)	SLC6A1	-1.46	0.0226
hsa-miR-141-3p	0.75	0.0111	TargetScan Human	Moderate (predicted)	RSAD2	-1.06	0.0253
hsa-miR-542-3p	1.34	0.0025	TargetScan Human	Moderate (predicted)	CAPN5	-0.95	0.0255
hsa-miR-424-5p	1.01	0.0034	Ingenuity Expert Findings	Experimentally Observed	KITLG	-1.26	0.0279
hsa-miR-15b-3p	0.70	0.0147	TargetScan Human	Moderate (predicted)	KITLG	-1.26	0.0279
hsa-miR-503-5p	1.52	0.0005	TargetScan Human	Moderate (predicted)	RGS5	-1.08	0.0323
hsa-miR-16-2-3p	0.85	0.0025	TargetScan Human	Moderate (predicted)	RGS5	-1.08	0.0323
hsa-miR-450b-5p	1.20	0.0025	TargetScan Human	Moderate (predicted)	RGS5	-1.08	0.0323
hsa-miR-424-5p	1.01	0.0034	TargetScan Human	High (predicted)	RGS5	-1.08	0.0323
hsa-miR-424-5p	1.01	0.0034	TargetScan Human	High (predicted)	RUNX1T1	-0.88	0.0323
hsa-miR-141-3p	0.75	0.0111	TargetScan Human	Moderate (predicted)	ITGA6	-0.92	0.0323
hsa-miR-542-5p	1.12	0.0111	TargetScan Human	Moderate (predicted)	ITGA6	-0.92	0.0323
hsa-miR-25-3p	0.61	0.0137	TargetScan Human	Moderate (predicted)	ITGA6	-0.92	0.0323
hsa-miR-15b-3p	0.70	0.0147	TargetScan Human	Moderate (predicted)	RGS5	-1.08	0.0323
hsa-miR-19b-3p	0.55	0.0157	TargetScan Human	Moderate (predicted)	RUNX1T1	-0.88	0.0323
hsa-miR-21-3p	0.95	0.0273	TargetScan Human	Moderate (predicted)	ITGA6	-0.92	0.0323
hsa-miR-21-3p	0.95	0.0273	TargetScan Human	Moderate (predicted)	RUNX1T1	-0.88	0.0323
hsa-miR-144-5p	0.65	0.0473	TargetScan Human	High (predicted)	RGS5	-1.08	0.0323
hsa-miR-503-5p	1.52	0.0005	TargetScan Human	Moderate (predicted)	PLAGL1	-0.96	0.0333
hsa-miR-16-2-3p	0.85	0.0025	TargetScan Human	Moderate (predicted)	PLAGL1	-0.96	0.0333
hsa-miR-424-5p	1.01	0.0034	TargetScan Human	Moderate (predicted)	PLAGL1	-0.96	0.0333
hsa-miR-942-5p	0.87	0.0092	TargetScan Human	Moderate (predicted)	ENTPD3	-1.68	0.0348
hsa-miR-135a-5p	-2.14	0.0004	TargetScan Human	High (predicted)	AKR1C1	1.73	0.0359
hsa-miR-451a	1.00	0.0014	TargetScan Human	Moderate (predicted)	OXCT1	-1.12	0.0377
hsa-miR-16-2-3p	0.85	0.0025	TargetScan Human	Moderate (predicted)	OXCT1	-1.12	0.0377
hsa-miR-503-5p	1.52	0.0005	TargetScan Human	Moderate (predicted)	SLIT2	-1.12	0.0394
hsa-miR-424-5p	1.01	0.0034	TargetScan Human	High (predicted)	SLIT2	-1.12	0.0394
hsa-miR-135a-5p	-2.14	0.0004	TargetScan Human	Moderate (predicted)	RARA	0.92	0.0403
hsa-miR-21-3p	0.95	0.0273	TargetScan Human	Moderate (predicted)	IL17RD	-1.15	0.0444

Figure S1

A



B



C

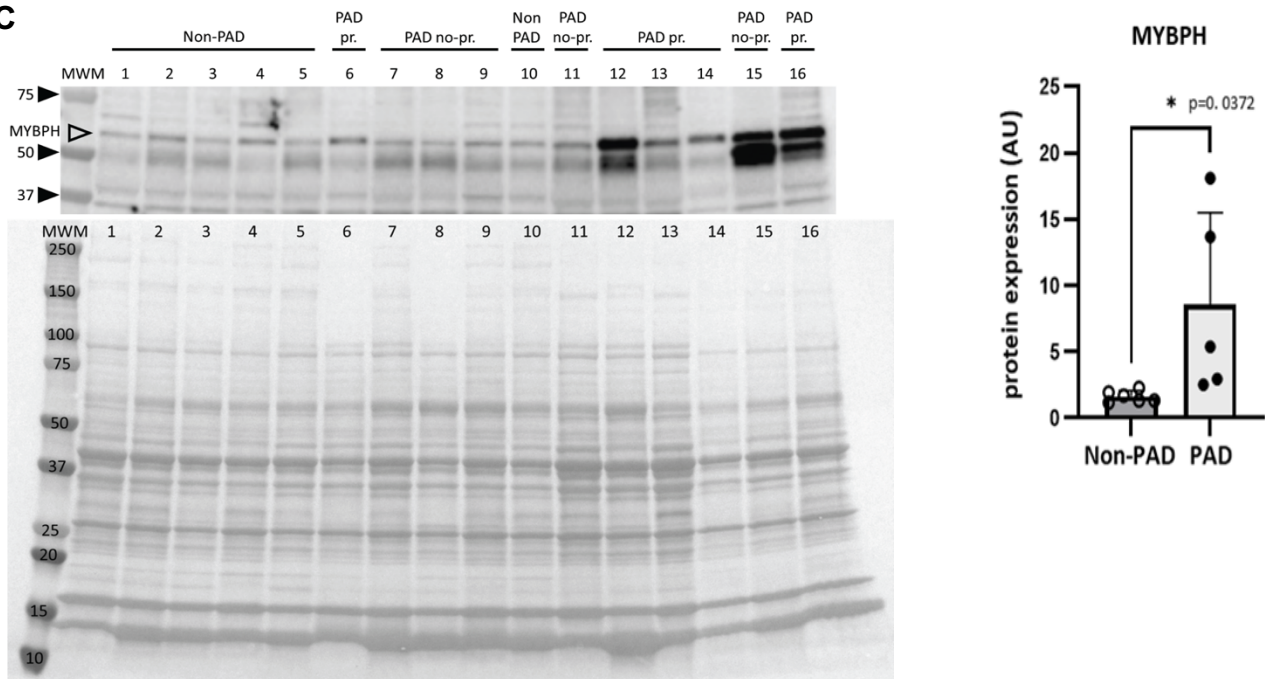


Figure S1. RT-qPCR analysis of top differentially regulated transcripts in non-PAD and PAD progression groups. (A) upregulated transcripts: CDKN1A, cyclin dependent kinase inhibitor 1A; PLA2G2A, phospholipase A2 group IIA; NNMT, Nicotinamide N-Methyltransferase; HES1, Hes Family BHLH Transcription Factor 1; ACTC1, Actin Alpha Cardiac Muscle 1; MYBPH, Myosin Binding Protein H; MYOG, myogenin; (B) downregulated transcripts: ITGA8, Integrin Subunit Alpha 8; XAF1, XIAP Associated Factor 1; INHBA, Inhibin Subunit Beta A; HAS2, Hyaluronan Synthase 2. (C) Western blot analysis of MYBPH (open arrow) with tissue lysate from skeletal muscle biopsies of

individuals without PAD (peripheral artery disease) and diagnosed with PAD; PAD pr.: PAD progression; PAD no-pr.: PAD no progression; MWM: molecular weight marker. 1-16: individual sample lanes (sample group indicated above).

Figure S2

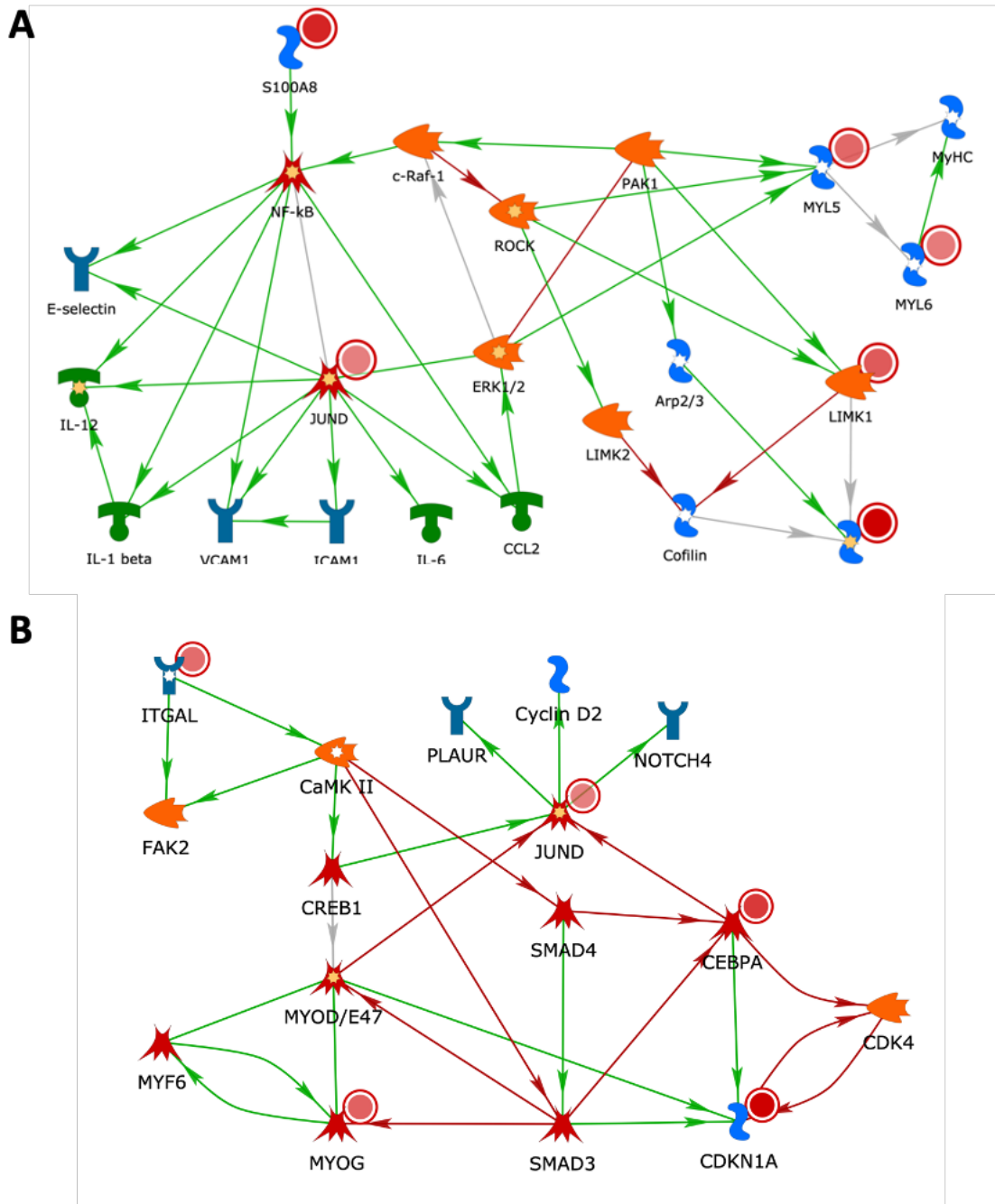


Figure S2. Visualization of gene networks of the “Inflammation Amphoterin signaling” (A) and “Signal Transduction TGF-beta, GDF and activin signaling” (B) pathways. Blue targets indicate downregulation; red targets indicate upregulation. S100A8, S100 calcium binding protein A8; NF-κB, NF-kappa B; c-Raf-1, proto-oncogene, serine/threonine kinase; PAK1, P21 (RAC1) Activated Kinase 1); MYL5, Myosin Light Chain 5; MyHC, Myosin heavy chain; MYL6, Myosin Light Chain 6; IL-12, interleukin-12;

VCAM1, vascular adhesion molecule-1; ICAM1, intercellular adhesion molecule-1; IL-6, interleukin-6; CCL2, C-C Motif Chemokine Ligand 2; ERK1/2, mitogen-activated protein kinase 1 and 2; LIMK2, LIM Domain Kinase 2; ARP2/3, Actin Related Protein 2/3; LIMK1, LIM Domain Kinase 1; ITGAL, Integrin Subunit Alpha L; CaMK II, Calcium/Calmodulin Dependent Protein Kinase II Alpha; PLAUR, Plasminogen Activator, Urokinase Receptor; CREB1, CAMP Responsive Element Binding Protein 1; JUND, Proto-Oncogene AP-1 Transcription Factor subunit; SMAD4, SMAD Family Member 4; CEBPA, CCAAT Enhancer Binding Protein Alpha; CDK4, Cyclin Dependent Kinase 4; MYOD, myoblast determination protein 1; MYF6, Myogenic Factor 6; MYOG, myogenin; SMAD3, SMAD Family Member 3, CDKN1A, Cyclin Dependent Kinase Inhibitor 1A.

Figure S3

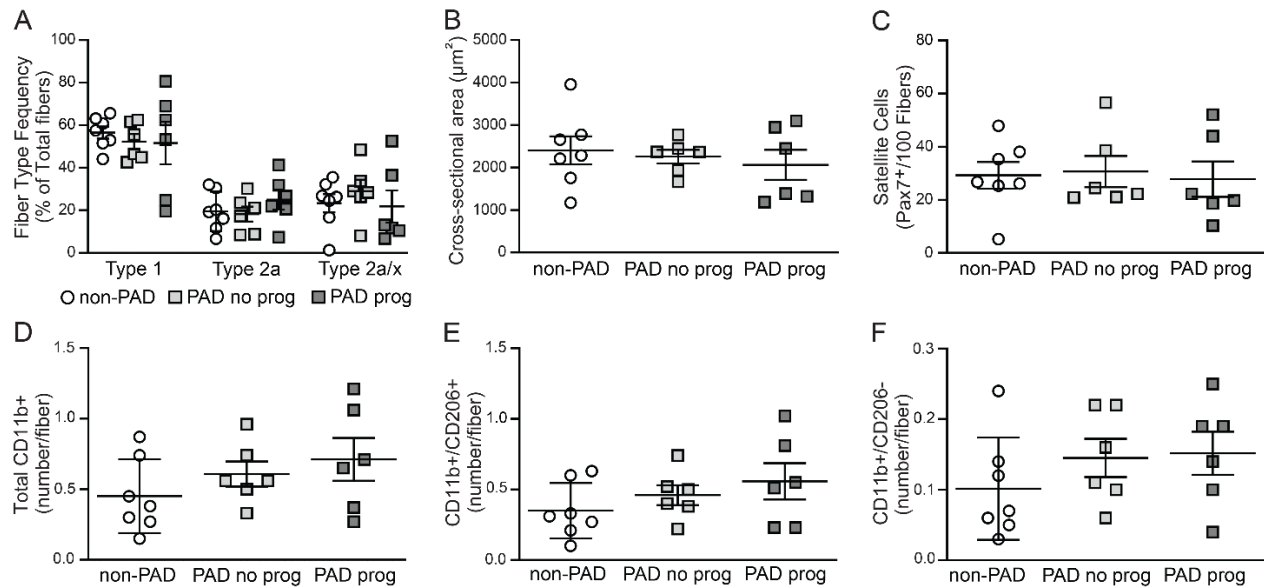
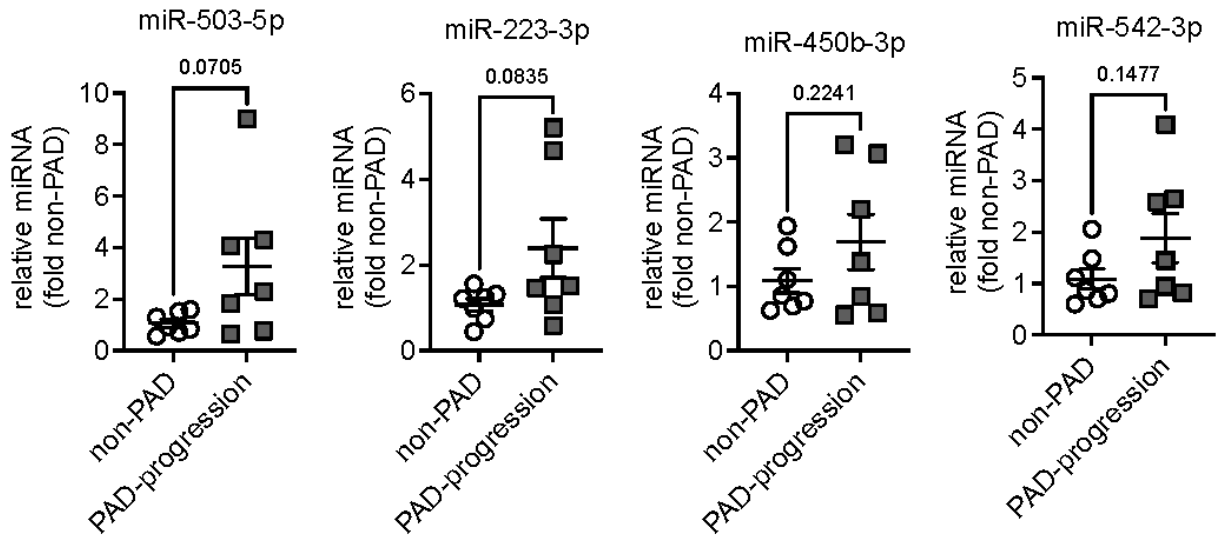


Figure S3. No difference in fiber type frequency, average fiber size, satellite cell abundance, or macrophage populations in gastrocnemius muscle from people with PAD (with or without progression) and non-PAD. A) Scatter plot showing the frequency of each fiber type (% of Total) within gastrocnemius muscle biopsies. Each circle or rectangle represents an individual subject, bars indicate mean \pm SEM. B) Average cross-sectional area for all muscle fibers measured within people without PAD (non-PAD; n=7), people with PAD without functional decline (PAD no prog; n=6) and people with PAD and functional decline (PAD prog; n=6). Each circle or rectangle represents an individual subject, bars indicate mean \pm SEM. C) Scatter plot showing quantification of satellite cell abundance. Satellite cells were identified as Pax7+ nuclei and data are expressed per 100 muscle fibers. Each circle or rectangle represents an individual subject, bars indicate mean \pm SEM. D-F) No difference in macrophage populations between groups, quantified using CD11b (pan macrophage marker) and CD206 (M2-like macrophage marker). Scatter plots show quantification of: D) total macrophages (total CD11b+), E) M2-like macrophages (CD11b+/CD206+) and M1-like macrophages (CD11b+/CD206-). Each circle or rectangle represents an individual subject, bars indicate mean \pm SEM. A-F) Groups are labeled as follows: subjects without PAD (non-PAD; n=7), subjects with PAD without functional decline (PAD no prog; n=6) and subjects with PAD and functional decline (PAD prog; n=6)

Figure S4

A



B

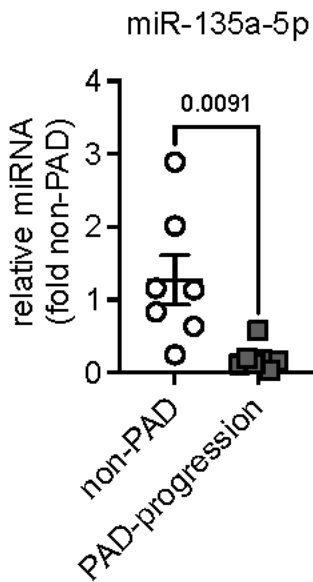


Figure S4. RT-qPCR analysis of top differentially regulated miRNAs in non-PAD and PAD progression groups. (A) upregulated miRNAs from RNA-seq; (B) downregulated miRNA from RNA-seq.

Figure S5

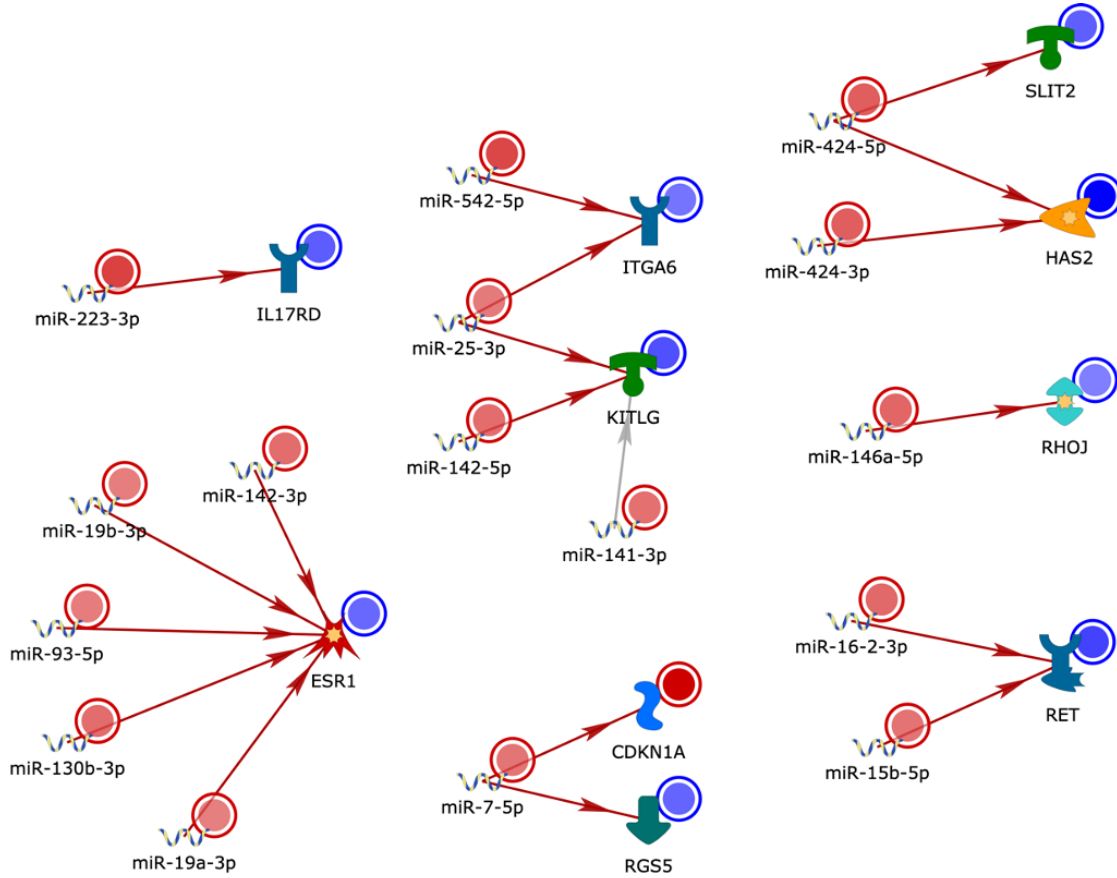


Figure S5. Significantly enriched interactions of miRNA and gene targets that are differentially expressed between PAD progression and non-PAD groups. Red dot indicates upregulated miRNA or gene and blue dot indicate downregulated gene or miRNA. IL17RD, Interleukin 17 Receptor D; ITGA6, Integrin Subunit Alpha 6; HAS2, Hyaluronan Synthase 2; KITLG, KIT Ligand; RHOJ, Ras Homolog Family Member J; ESR1, Estrogen Receptor 1; CDKN1A, Cyclin Dependent Kinase Inhibitor 1A; RGS5, Regulator Of G Protein Signaling 5); RET, Ret Proto-Oncogene.